Design of a Blended Wing Body Aircraft

A project present to
The Faculty of the Department of Aerospace Engineering
San Jose State University

in partial fulfillment of the requirements for the degree
Master of Science in Aerospace Engineering

By

Randhir Brar

December 2014

approved by

Dr. Nikos Mourtos
Faculty Advisor

San José State
UNIVERSITY

ABSTRACT

Blended wing body (BWB) aircraft is more than an idea. NASA in a joint venture with Boeing, has recently completed a highly successful and productive flight test program of experimental BWB aircraft. These successful flight tests have opened the doors for the further development of BWB aircraft for potential full-scale commercial aircraft in future. Being very efficient and quiet, the BWB has shown promise for meeting all of NASA's environmental goals for future aircraft designs. This configuration incorporates design features from conventional fuselage as well as traditional flying wing. In this concept, wide airfoil-shaped body is smoothly blended with high lift wings, which means that the entire aircraft contributes to the generation of lift thereby potentially increasing fuel economy and range, while at the same time, massive increase in internal payload is obtained. This report presents the preliminary design of large transport blended wing body aircraft capable of carrying 586 passengers, with range more than 9000 miles. It is also intended for required mission aircraft to meet FAR 25 requirements.

ACKNOWLEDGMENT

I would like to thank all people including family members, teachers and friends who supported and motivated me throughout my graduate studies.

First, I would like to express my sincere gratitude to my advisor Dr. Nikos Mortous. His guidance has helped me not only in this project but throughout my graduate program. Without his technical and personal support, this project would not have been possible. He is simple, humble and welcoming to students for any problem. I could not have imagined better advisor to my master program.

Second, I want to acknowledge my brother Manpreet Brar and sister in-law Manbir Brar for their unequivocal support and motivation throughout my studies.

Third, my deepest gratitude goes to my parents, Mohinder Singh and Jeet kaur for their love and care. Throughout the hardships in my life, they always stood by me and helped me. I still remember those sleepless nights my father worked to financially support mine and my brother's education. And I cannot express enough thanks to my mother with just words. She is simply awesome. All the credit goes to my parents for what I am today.

Above all, I would like to thank my wife Preet Brar for her personal support and great patience at all times. My mere words cannot express kind of support and motivation I got from her. She suffered a lot, worked double shifts to support our living and I can never pay her back for what she did for me. I appreciate her for maintaining patience during phases I was not able to give her time because of my busy study schedule.

Last, but not the least, I would like to thank almighty God. I do not exist without him and I always believe that whatever he does or happens with me is for my betterment.

The Designated Committee Approves the Project Titled

PRELIMINARILY DESIGN OF BLENDED WING BODY PASSENGER AIRCRAFT FOR
LONG RANGE

By

RANDHIR BRAR

APPROVED FOR THE DEPARTMENT OF AEROSPACE ENGINEERING SAN JOSE STATE
UNIVERSITY

May 2014

Dr. Nikos Mortous   Committee Chair, San Jose State University

TABLE OF CONTENTS

LIST OF TABLES

LIST OF FIGURES

ABBREVIATIONS

BWB	Blended Wing Body
GMF	Global Market Forecast
NASA	National Aeronautics and Space Administration
NACA	National Advisory Committee for Aeronautics
NOX	Nitrogen oxide
FAA	Federal Aviation Administration
FAR	Federal Aviation Regulations
MTOW	Maximum take-off weight
LCD	Liquid crystal display
MLW	Maximum landing weight
MZFW	Maximum zero fuel weight
MCW	Maximum cargo volume
AR	Aspect Ratio
SC	Service ceiling
AAA	Advanced Aircraft Analysis
CG	Center of Gravity
AC	Aerodynamic Center
CAD	Computer Aided Design
BLI	Boundary Layer Ingestion
MAC	Mean Aerodynamic Chord
HP	High pressure
LP	Low pressure
SC	Service ceiling
RC	Climb rate

NOMENCLATURE

Symbol	Definition
W_{PL}	Airplane Payload
V	Airplane Speed
R	Airplane Range
L_a	Airplane overall length
W_{TO}, W	Airplane take-off weight
W_E	Empty weight
C_j	Specific fuel consumption
L	Lift
D	Drag
R_{CR}	Cruise Range
E_{LTR}	Loiter time in hours
W_{FF}	Fuel weight fraction of total mission
W_{F_USED}	Usable Fuel weight during mission
$W_{RESERVE}$	Weight of reserve fuel
W_F	Weight of mission fuel
W_{E-tent}	Tentative empty weight of airplane
$W_{TO-GUESS}$	Guessed take of weight
$W_{E-allow}$	Allowed empty weight
M_{tfo}	Mass fraction of trapped fuel and oil
CR	Cruise
LTR	Loiter
C_L	Lift coefficient
C_{Lmax}	Maximum Lift coefficient of airplane (clean)
C_{Lmax-l}	Maximum Lift coefficient of airplane during landing
C_{l-max}	Maximum Lift coefficient of airfoil
$C_{mc/4}$	Pitching moment coefficient at quarter chord
$(L/D)_{max}$	Maximum Lift to Drag Ratio
α	Angle of attack

Symbol	Description
b	Wing span
S	Wing reference area
λ	Taper ratio of wing
$\bar{c}$	Mean aerodynamic chord
C_1	Root chord of inboard wing
C_2	Tip chord of inboard wing and root chord outboard wing
S_1	Reference area inboard wing
S_2	Reference area outboard wing
b_1	Span inboard wing
b_2	Span outboard wing
Λ	Sweep angle
n_s	Number of landing gear strut
P_m	Maximum static load per strut of main gear
P_n	Maximum static load per strut of nose gear
C_{m_0}	Pitching moment coefficient
M	Rate of change of moment coefficient with respect to α
M_{cg}	Pitching moment coefficient at zero angle of attack
M_{ac}	Pitching Moment
h	Pitching Moment about CG
h_0	Pitching Moment about AC
L_w	Distance of CG from the leading edge of wing
h_t	Distance of AC from leading edge of wing
C_{Lw}	Lift generated by wing
L_t	Distance of tail AC from leading edge of wing
i_t	Wing lift coefficient
S_t	Lift generated by tail
a_w	Angle of attack of Horizontal tail
K_n	Tail reference area
V_c	Lift Coefficient slope of wing
	Static margin
	Vertical component of velocity

e	Span efficiency
ϕ	Twist angle of wing
Xu	Axial force due to velocity
Xw	Axial force due to incidence
Zu	Normal force due to velocity
Zw	Normal force due to downwash lag
Zq	Normal force due to pitch rate
Mu	Pitching moment due to velocity
Mw	Pitching moment due to incidence
Mq	Pitching moment due to pitch rate
Yv	Side force due to side slip
Yp	Side force due to roll rate
Yr	Side force due to yaw rate
Lv	Rolling moment due to side slip
Lp	Rolling moment due to roll rate
Lr	Rolling moment due to yaw rate
Nv	Yawing moment due to side slip
Np	Yawning moment due to roll rate
Nr	Yawning moment due to yaw rate
Xde	Axial force due to elevator
Yda	Side force due to aileron
Zde	Normal force due to elevator
Lda	Rolling moment due to aileron
Mde	Pitching moment due to elevator
Ndr	Yawning moment due to rudder
u	Velocity of aircraft along body axis
w	Velocity of aircraft perpendicular to body axis
q	Pitch rate
Θ	Pitch angle
ζ	Damping ratio
ω	Un-damped natural frequency

v	Velocity of aircraft along lateral axis
p	Roll rate
r	Yaw rate
ϕ	Roll angle
φ	Yaw angle
	Elevator deflection

1.0 Introduction

The conventional aircraft design with fuselage and wing is the most persuasive concept in the aviation industry. This design concept has existed since very first powered flight by wright brothers' flyer in 1903. Although many design changes have been made throughout the first century of powered flight to improve performance, but even most of today's aircraft has conventional design; tube and wing as a core. In conventional configuration, both fuselage and wing play separate roles: fuselage carries payload and wings generate lift. The conventional design is well proven and its aerodynamic efficiency has been increased over the period of time. With more than a century of continuous development, conventional design has reached the stagnation point, leaving very little scope for further improvement in efficiency. The hiking fuel prices and environmental concerns are forcing the aviation industry to look into the new revolutionary concept for high fuel efficiency.

The Blended Wing Body (BWB) configuration is the future of aviation that can offer very high fuel economy along with large payload and quieter & cleaner operation. It is the hybrid shape, with fuselage and wings blended smoothly to make a single lifting surface. The BWB resembles a flying wing, but also incorporates features from conventional aircraft. This combination gives several advantages over conventional tube and wing airframes. As airframe encompasses airfoil shape body blended with the high lift wings, it allows the whole airframe to generate lift that improves the fuel economy. It is expected that BWB aircraft would improve lift to drag ratio by 50 % and fuel efficiency by 20 to 25 % in comparison to conventional configuration [2].

The primary objective of this report is to design a large BWB transport aircraft that has seating capacity of 586 passengers and is capable of achieving transcontinental flights.

1.1 Motivation

The first half century of powered flight was mainly concerned about flying longer, faster and higher. In the latter half of century, focus started to shift slowly towards the need of transport with high fuel efficiency, and less noise. In modern world, high efficiency, low noise and cleaner operation became the priority due to increasing fuel prices and environmental concerns. The BWB is one of the promising alternatives which can meet the demands of the present and future aviation. The BWB configuration offers several advantages over conventional tube and wing configuration [2].

   a. Reduction in weight by 10-15 %.

   b. Increased fuel efficiency by 20-25 %.

   c. Reduction in noise by placing engines on the top of the wings.

   d. Increased L/D by 50 %.

   e. Reduction in NOX emission BY 17 %.

   f. Reduction in operating costs by 10-15%.

   g. Large payload volume for the same size of the aircraft.

The primary motivation for this project came from the success of the flight test program of X-48C by NASA and Boeing, which ended in April 2013 [16].This eight-month long flight-test program explored and validated the aerodynamic characteristics of the BWB design concept. Test results have shown that a BWB aircraft offers a tremendous promise for greater fuel efficiency and reduced noise. It can be controlled as effectively as a conventional tube-and-wing aircraft during takeoffs, landings and other low-speed segments of the flight regime [16].

Also, in recent years, the increased demand of air travel resulted in problems like heavy air traffic, terminal congestion and parking facilities. Large airliner is the demand of time, to carry

more passengers while restricting the number of operations from airports. The quest for more people on fewer aircraft has been defined by NASA as "The Lure of Large Aircraft" [2].

Need of high performance, quiet and cleaner aircraft along with the lure of large aircraft is the overall motivation to design large long haul passenger BWB aircraft. In this report, the required mission aircraft is named as BWB 601.

1.2 Mission Specifications

1.2.1 Range

The BWB 601 aircraft is required to fly intercontinentally and must be capable of achieving world longest flights nonstop. BWB 601 will fly the routes listed in table 1.

Range of BWB 601 = Longest route listed in table 1 + Reserve range

Based on required maximum flight distance and reserve range, the range of BWB 600 was decided to be 9800 miles.

Table 1: Routes of BWB 601

From	To	Distance (miles)
Sydney	Dallas	8,578
Johannesburg	Atlanta	8,439
Dubai	Los Angeles	8,339
Dubai	Brisbane	8,303
Dubai	Houston	8,168
Dubai	San Francisco	8,103

1.2.2 Payload

Payload includes the weight of passengers, crew, flight attendants and baggage. The mission designed aircraft will carry 586 passengers. A standard number of 3 crew member are required for aircraft operation. The number of the flight attendants depends upon the number of passengers as per FAA regulations. According to FAR section 121.391:

"For airplanes having seating capacity of more than 100 passengers, two flight attendants plus an additional flight attendant for each unit (or part of a unit) of 50 passenger seats above a seating capacity of 100 passengers".

Therefore for 586 passengers, a minimum of 12 flight attendants are required. For calculation purposes, the standard weight of each person is taken 180 lbs. and baggage 30 lbs. per person. Total payload will be 123060 lbs.

1.2.3 Speed

The maximum speed of subsonic airplane is limited by drag divergence Mach number. At the drag divergence point, drag force on aircraft rises drastically due to transonic effects. It is desired for BWB 601 to fly at maximum possible subsonic cruise speed without entering in drag divergence Mach effects. From the comparison of aircraft with similar mission profile, it was decided that the BWB 601 will fly at a cruise speed of Mach 0.85 and will have a maximum speed of Mach 0.92.

1.2.4 Service Ceiling

The maximum service ceiling of BWB 601 will be 45000 ft.

1.2.5 Climb Rate

The rate of climb will be 4500 ft. /min.

1.2.6 Takeoff and Landing Distance

The takeoff and landing distance may seem as performance characteristics of secondary importance, but they are often very crucial from design point of view. It is desirable for the aircraft to meet take-off field length requirements for selected airports with a full payload and fuel. Large passenger aircraft of similar size as that of BWB 601, have takeoff distances at MTOW in the range of 10,000 ft. and landing distance of 7000 ft. Shortening of these distances, while not a requirement, is a preferred outcome of the BWB 601 model. Specifically, a decrease in takeoff distance as in BWB configuration, offers a high lift to drag ratio.

1.3 Critical Mission Requirements

To be a competitor to similar mission profile airplanes like Airbus 380-800 and Boeing 747 8I, there are some critical mission requirements which must be met. Table 2 lists the critical mission requirements.

Table 2: Critical mission requirements

Cruise speed	0.85 Mach
Maximum speed	0.92 Mach
Range	9800 miles
No of passengers	586

1.4 Sketch of the Mission Profile

The sketch of mission profile of BWB 601 is shown in a Fig 1.
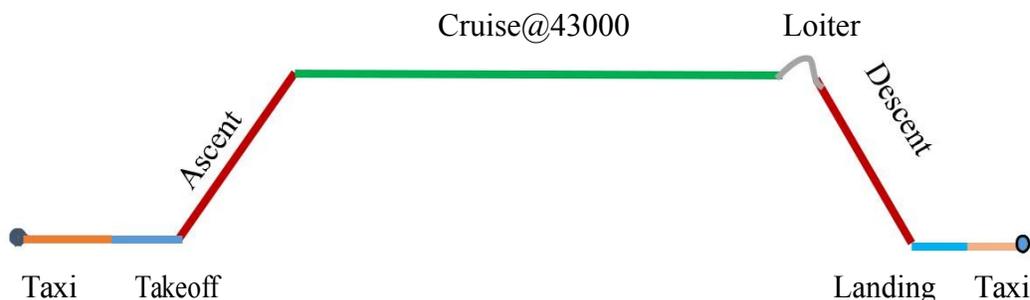
Figure 1: Mission Profile of BWB 601 aircraft

1.5 Market Analysis

Air traffic is increasing every day due to economic growth, affordability, ease of travel, urbanization and tourism. According to Airbus' latest Global Market Forecast (GMF), in the next two decades (2013 -2032), air traffic will grow at 4.7 percent annually requiring over 29,220 new passenger aircraft [22]. According to this rate, the worldwide aircraft fleet will double by 2032. Meanwhile, airspace and airport congestion are becoming serious problems in aviation. Saturated airspace is increasing the probability of disasters due to human errors or malfunctioning of communication satellites. The airspace congestion also has been identified as the reason for 60 % of delays that the airspace congestion, large transport aircraft could be the option to limit the number of increasing flights.

According to GMF, in a very large aircraft segment dominated by the A380, there is a requirement for conventional tube travelers encounter everyday [2]. In order to tackle problems due to the rising additional profitability to airliners as discussed in section 1.1.

	Airbus A380-800	Boeing 747 8I	Ann 225 mriya	Boeing X-48
Maximum structural payload	89,200 kg (196,700 lb)	169,100 lb (76,700 kg)		
Maximum cargo volume	184 m³ (6,500 cu ft)	5,705 cu ft (162 m3)	1,300m3	
Cruising speed	Mach 0.89 (945 km/h, 587 mph)	Mach 0.855 (570 mph/917 km/h)	800 km/h (497 mph; 432 kn)	
Maximum speed at cruise altitude	Mach 0.96 (at cruise altitude: 1020 km/h, 634 mph	Mach 0.855 (570 mph/917 km/h; 495 kn)	850 km/h (528 mph; 459 kn)	
Take off run at MTOW/SL ISA	2,950 m (9,680 ft)			
Range at design load	15,700 km (8,500 nmi, 9,755 mi)	8,000 nmi (9,210 mi; 14,800 km) at MTOW with 467 passengers and baggage	15,400 km (9,569 mi; 8,315 nmi) with maximum fuel; range with maximum payload: 4,000 km (2,500 mi)	
Overall length	72.73 m (238.6 ft)	250 ft 2 in (76.3 m)	84 m (275 ft 7 in)	
Height	24.45 m (80.2 ft)[185]	63 ft 6 in (19.4 m)	Height: 18.1 m (59 ft 5 in)	
Outside fuselage width	7.14 m (23.4 ft)			
Outside fuselage height	8.41 m (27.6 ft)			
Wingspan	79.75 m (261.6 ft)[	224 ft 7 in (68.5	88.4 m (290 ft 0 in)	

		m)	

1.6 Economic Feasibility

The BWB airplane is considered to be the next generation airliner. The BWB concept is extremely fuel efficient along with other benefits which includes lower operating costs, lower production costs, reduced airport or airspace congestion, lower fares, reduced environmental impact and improved safety [2]. Fuel efficiency improvement comes from the fact that BWB will have higher lift to drag ratio. Improved efficiency will directly impact the operating cost and ticket fair. Lower production cost is predicted from the fact that BWB body will not involve many tight bends, so manufacturing cost will go down. It is believed that this design concept has more crash survivability than the conventional design [2]. Reduced airport or airspace congestions have already been discussed in previous sections.

Although BWB possesses huge future potential but it should be noted that this concept is still at inception stage. The practical cost related with this project involves costs of research, development, design, testing, safety assessment, certification procedure and maintenance. In order to be commercially successful, mass production of BWB aircraft is required which is a long way journey. But again, as discussed in market analysis section, BWB long haul transport have very good potential market, so can be brought to mass production. Looking at the advantages it can offer, along with reasonable market demands, building such aircraft seems will worth.

1.7 Constraints

Some of challenges or constraints faced by BWB configuration are structures and materials, controls, propulsion-airframe integration, systems integration, emergency evacuation and social issues.

Aircraft structure carries aerodynamic loads, weight and cabin pressure loads. The cabin internal pressure loads are carried more efficiently by cylindrical shape (in hoop tension) as in case of conventional aircraft. BWB has non-cylindrical fuselage which makes it hard to carry internal pressure loads and requires heavier structure [4]. There is a need of developing new composite material like graphite stitched epoxy resin, which is stronger enough to carry cabin loads without additional weight [2].

Another important question to ask is- where the windows will be placed in BWB configuration? In this design, there will be only a few passenger windows at the front section and rest of the seats will have multi-functional LCDs for outside views. It is interesting to see how people will get used to such concept. Also according to FAR 25 requirements, passenger aircraft should have that many emergency exits such that it can be evacuated in 90 seconds in case of emergency. In BWB aircraft, fuselage is blended with wings which leave little space on sides of the center body for emergency exits. In order to overcome this issue, emergency exits should be placed on the bottom or top sides of center body.

The lack of conventional tail possesses potential longitudinal and control deficiencies. Tailless aircraft imposes design challenges to obtain required stability and control. However, by using advanced digital flight controls and envelope limits concepts, such design challenges can be met.

BWB configuration also affects the landing approach speed and attitude [29]. The trailing-edge control surfaces flaps cannot be used because the airplane has no tail to trim the resulting pitching moments. Trailing-edge surface deflection is set by trim requirements, rather than maximum lift. This will result in lowering the maximum lift coefficient of a BWB than that of a conventional configuration, and, hence, the wing loading of a BWB will be lower. Also, lack of flap means that the maximum lift coefficient for BWB will occur at a relatively large angle of attack and the flight attitude during approach will be correspondingly high.

Last but not the least, people have been used to the fuselage wing concept for almost ten decades and it will take some time to get them into an unconventional one.

2.0 Literature

2.1 Blended Wing Body Related Concepts

Throughout the history, researchers tried to design several aerodynamically efficient concept aircraft such as flying wing and other tailless aircraft. Some of these aircraft related to the blended wing body from history are discussed in this section.

2.1.1 Burnelli RB-1

In 1921, the concept of airfoil shaped fuselage to increase lift was patented by pioneering aviator Vincent Justus Burnelli [6]. Later on, he designed an aircraft named RB-1, which was a twin biplane airliner with lifting body. The body contributed about 27 % of the total lifting area and was designed to support about 15 % of its weight [6]. First flight of RB-1 on 21 June 1921 showed good performance. However, the first model produced was badly damaged while on the ground during a storm.

Figure 2: Burnelli RB-1 [5]

Table 3: Technical specifications of RB-1 [5][6]

Crew [11]	**2**
Capacity	30
Length	41 ft 2 in
Wingspan	74 ft
Height	18 ft
Empty weight	8137 lb.
Gross weight	14637 lb.

2.1.2 Westland Dreadnought

The Westland dreadnought was the experimental aircraft built by Bristol Aeroplane Company Limited in 1924. This project was aimed to trail the aerodynamic wing and fuselage design of Woyevodsky [25]. This aircraft crashed in its very first flight severely injuring the pilot. Mission was aborted after this incident and no further aircraft was made [25].
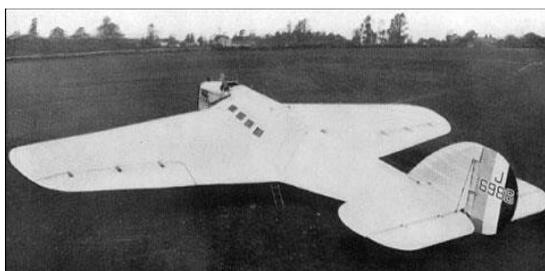
Figure 3: Westland Dreadnought [32]

Table 4: Technical specifications of Westland Dreadnought [32]

Crew	**2**
Capacity	8
Length	56 ft
Wing span	69 ft 3 in
Wing area	840 ft^2

2.1.3 Northrop YB-49

The Northrop YB-49 was a purely flying wing jet powered heavy bomber aircraft developed by Northrop Corporation in 1947 [19]. This aircraft had four vertical stabilizers: two on each wing, installed on both sides of the jet engine exhausts. To minimize the flow in span wise direction, the wings were fitted with four air dams extending forward from the vertical stabilizer. Flight testing showed good performance; however, stability issues during simulated bomb runs along with some political issues doomed the flying wing [19]. Although this aircraft was unsuccessful, but it laid the foundation for the development of B-2 stealth fighter.
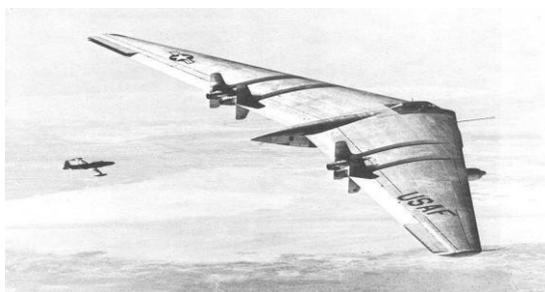
Figure 4: Northrop YB-49 [19]

Table 5: Technical specifications of Northrop YB-49 [19]

Crew	**7**
Length	53.08 ft
Height	20.28 ft
Wing span	172 ft
Wing area	4000 ft^2

2.1.4 Northrop B-2 Stealth Bomber

The B-2 spirit, also known as stealth bomber was developed in 1989 by Northrop Grumman Corporation to have a less exposable cross section to radar [33]. The B-2 design falls between classic flying wing and the BWB concept. It is usually classified as a flying wing, as the protruding body sections are not much larger than the underlying wing shape structure. B-2 is revolutionary from an aeronautics perspective: being efficient can cover long ranges without refueling. It does not have any of the standard stabilizing systems, but flying qualities matches very well with conventional aircraft.

Figure 5: Northrop B-2 stealth fighter [33]

Table 6: Technical specifications of Northrop B-2 Stealth fighter [33]

Crew [14]	**2**
Length	68.56 ft
Height	16.73 ft
Wing span	170.9 ft

2.2 Blended Wing Body Prototype Aircraft

In 1994, NASA and McDonnell Douglas initiated BWB research under the project named Advanced Concepts for Aeronautics (ACP) [7]. Under this project, they studied airliner designs of BWB configuration, which was essentially a flying wing with a wide lifting-body shaped center fuselage. In 1997, a small propeller-driven BWB model airplane of 5.2 m (17 ft) wingspan was built, and test-flown to demonstrate the flying characteristics [7]. The ACP studies ended in 1998 with revolutionary conclusions such as increase in L/D drag ratio, reduction in take-off gross weight and reduction in operating costs [7]. NASA and Boeing continued their BWB research and

in early 2000, Boeing began the construction of the BWB-LSV- an unmanned, 14% scale vehicle of the BWB transport, to evaluate the design in actual flight tests [23]. Later on in 2001, this project was named as X-48.

2.2.1   Boeing X-48

The Boeing X-48 is a BWB, experimental unmanned aerial vehicle, developed by NASA and Boeing to investigate feasibility of large BWB airliner. During the last decade, various X-48 models have been developed, followed by a series of ground and flight tests. According to NASA, X-48 design holds a very good promise of efficient large passenger aircraft. The variants of the X-48 investigated by NASA are discussed in following sections.

2.2.1.1 X-48A

The X-48A was primarily made of composites, had a wing span of 10.7 m and was powered by three small Williams J24-8 turbojets [23]. This was the small scaled model project which started in 2001 and it was expected to complete ground tests in 2003 [23]. However, the project was cancelled in 2002 due to some technical problems in the flight control system along with changing priorities of NASA.

Figure 6: Boeing X-48 A [23]

Table 7: Technical specifications for X-48 A [23]

Length	**?**
Wingspan	10.7 m (35 ft)
Weight	1130 kg (2500 lb.)
Speed	265 km/h (165 mph)
Ceiling	?
Propulsion	3x240 lb. Williams J24-8 turbojet

2.2.1.2 X-48B

After the cancellation of the X-48A in 2002, Boeing contracted Cranfield Aerospace (UK) to design and build a smaller BWB model [23]. In 2005, this BWB was designated as X-48B. The X-48B was remotely controlled aircraft, built to 8.5 % scale model of potentially flying aircraft [23]. Extensive ground tests were conducted in 2006, to validate engine, fuel system, battery endurance, the telemetry link, the flight-control software, and the aircraft's taxing characteristics [23]. Phase I flight tests were conducted at NASA's Dryden Flight Research Center in early 2007 to determine low speed, low altitude characteristics including engine out, stall and handling characteristics [18]. Phase II high speed flight tests took place in spring 2008 on modified X-48B. By April 2009, fifty X-48B flights had been completed successfully [23]. Flight tests demonstrated that BWB can aircraft can be flown as safely as current transport having traditional fuselage, wings and tail configuration.

Figure 7: Boeing X-48 B [18]

Table 8: Technical specifications for X-48 B [23] [4]

Length	?
Wingspan	6.22 m (20 ft 5 in)
Weight	225 kg (500 lb.)
Speed	220 km/h (120 knots)
Ceiling	3000 m (10000 ft)
Propulsion	3x Jet Cat P200 turbojet

2.2.1.3 X-48C

The X-48C was updated version of the X-48B, with some modifications, to reduce the noise level and for better stability controls [18]. Modifications included reducing the number of engines to two, and adding two vertical fins to shield the engine noise. Three 50-pound thrust jet engines of X-48B's were replaced with two 89-pound thrust engines [18]. Also, it was equipped

with modified flight control system software which included flight control limiters to keep the aircraft flying within the safe flight envelope. The X-48 C retained most dimensions of B model. The aft deck of the aircraft was extended about two feet to the rear and wing span increased by one inch. The X-48C was aimed to evaluate the low-speed stability and control of a low-noise version of a BWB aircraft. This aircraft made its first successful flight on Aug. 7, 2012 at Edwards Air Force Base [18].

The success of X-48 mission has proved that BWB configuration offers significantly greater fuel efficiency and reduced noise, can be controlled as effectively as a conventional tube-and-wing aircraft during takeoffs, landings and other low-speed segments of the flight regime [18].

Figure 8: Boeing X-48C [18]

Table 9: Technical specifications for X-48 C [23] [18]

Length	?
Wingspan	6.25 m (20 ft 6 in)
Weight	225 kg (500 lb.)
Speed	220 km/h (120 knots)
Ceiling	3000 m (10000 ft)
Propulsion	2x SPT15 Jet Cat Ducted Fan

2.3 Comparative Studies of Airplanes with Similar Mission Profile

Table 10 shows the tabulated comparisons of similar mission profile aircraft. Antonov AN-225 Mriya is the world largest commercial aircraft in-operation [9]. The AN-225, is powered by six engines, three per wing and has two tails. Dimensions of AN-225 are mind blowing with fuselage of 275 ft and wing span of 290 ft [9]. Also, maximum takeoff weight is an unbelievable 1,323,000 pounds. Ann 225 is cargo aircraft while the other three listed in table are passenger airliners.

Boeing 747-8I is slightly longer than the Airbus A380-800, with 250 ft 2 inch length compared to 245 ft length of the A380-800. However, the A380-800 is taller, has a larger wingspan and more maximum takeoff weight compared to B747-8I. Also A380-800 has the largest passenger capacity in the world. The boing 747-400 is little smaller in length however it is best-selling airplane in 747 series. For more detailed comparison, see table 10.

Table 10: Comparison of Long haul passenger airplanes with similar mission profile [17][9]

	A380-800	747-400	747 8I	Ann 225
Crew	2	2	2	6
Seating capacity	855(Maximum) 525-555 (3-class)	660 (Maximum) 416 (3-class)	605(maximum) 467 (3-class)	N/A
MTOW (lbs.)	1,268,000	910,000	987,000	1,410,958
MLW (lbs.)	869,000		688,000	
MZFW (lbs.)	814,000		651,000	
MCV (ft^3)	6,500		5,705	45909
Cruising speed	Mach 0.89	Mach 0.855	Mach 0.855	Mach 0.653
Maximum speed	Mach 0.96	Mach 0.92	Mach 0.855	Mach 0.694
Take-off distance (ft)	9,680	10,200		

Range (miles)	9,755	8826	9,210	9,569
Overall length (ft-inch)	245-0	231-10	250-2	275-7
Height (ft-inch)	80-0	63-8	63-6	59-5
Outside width (ft-inch)	23-5			
Outside fuselage height (ft-inch)	27-7			
Wingspan (ft-inch)	261-7	211-5	224-7	290
Wing area (ft^2)	9,100	6027.78		9,740
Aspect ratio	7.5	7.4		8.6
Service ceiling (ft)	43,097	43,000	43,000	36,089
Engines	4xTrent 900	4xPW 4062 4xGE CF6-80C2BF5	4xGEnx-2B67	6 × ZMKB
Thrust	75,000 lbf	4x63,300 lbf 4x62100 lbf	4x66,500 lbf	51,600 lbf

2.4 Three Dimensional Views of Aircraft with Similar Mission Profile
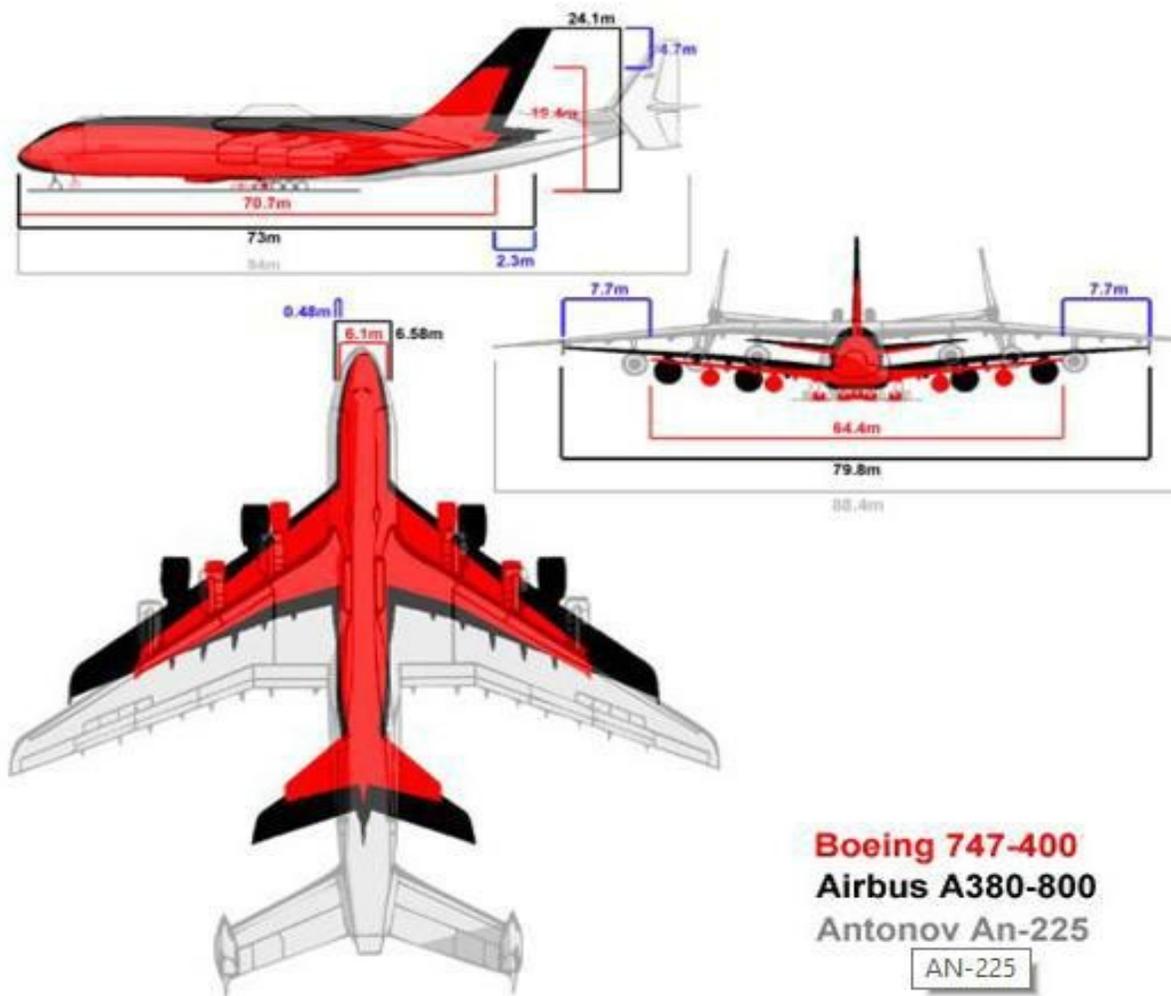
Figure 9: 3D Views of 747-400, A380-800 and AN-225 [9]
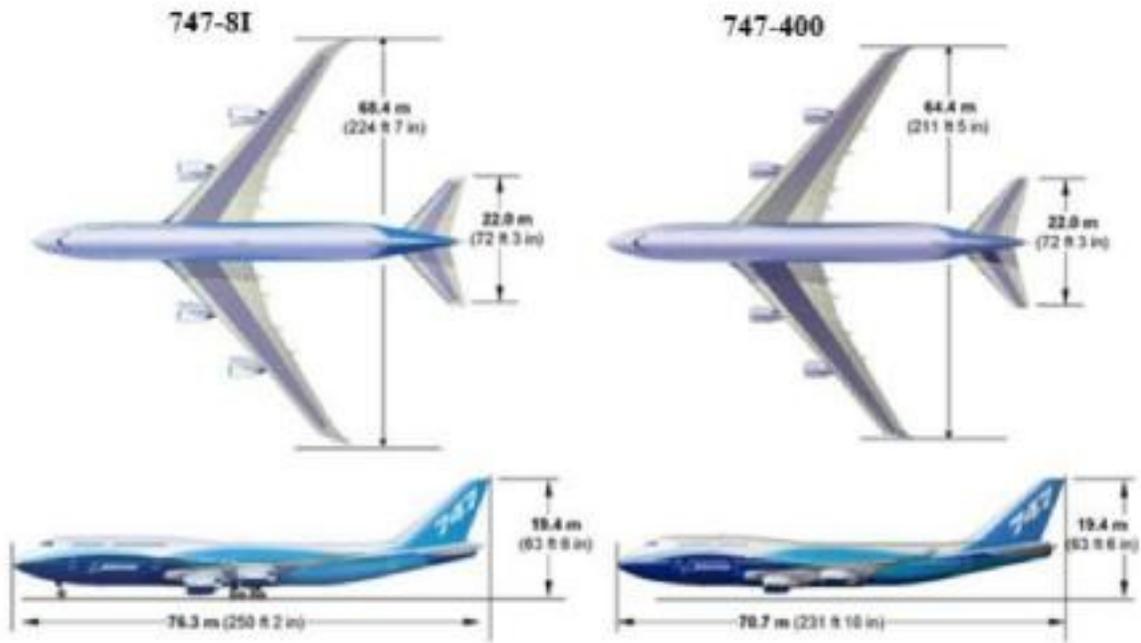
Figure 10: 3 D Views of 747-8I and 747-400 [31]

3.0 Mission Weight Estimates

3.1 Data Base for Takeoff Weights and Empty for Long Haul Transport Jets

Table 11: Data base for airplanes with similar mission profile [17] [9][31]

Aircraft	W_{TO} (lbs.)	W_E (lbs.)	Log_{10} (W_{TO})	Log_{10} (W_E)
Boeing				
747-400 ER	910,000	406,000	5.959041392	5.608526034
747-400	875,000	394,088	5.942008053	5.595593211
747-100	735,000	385,000	5.866287339	5.58546073
747-200	833,000	383,000	5.920645001	5.583198774
747-300	833,000	392,800	5.920645001	5.594171479
767-400 ER	450,000	229,000	5.653212514	5.359835482
777-200 LR	766,000	326,000	5.88422877	5.5132176
777-300	660,000	353,000	5.819543936	5.547774705
777-300 ER	775,000	366,940	5.889301703	5.564595057
787-9	540,000	254,000	5.73239376	5.404833717
Airbus				
A 380-800	1,235000	608,400	6.091666958	5.784189205
A 340-600	811,300	392,000	5.909181476	5.593286067
A 340-500	820,100	376,800	5.913866812	5.576110894
A 340-300	606,000	285,000	5.782472624	5.45484486
A 330-300	507,000	267,200	5.705007959	5.426836454

3.2 Log-log plot for weight data
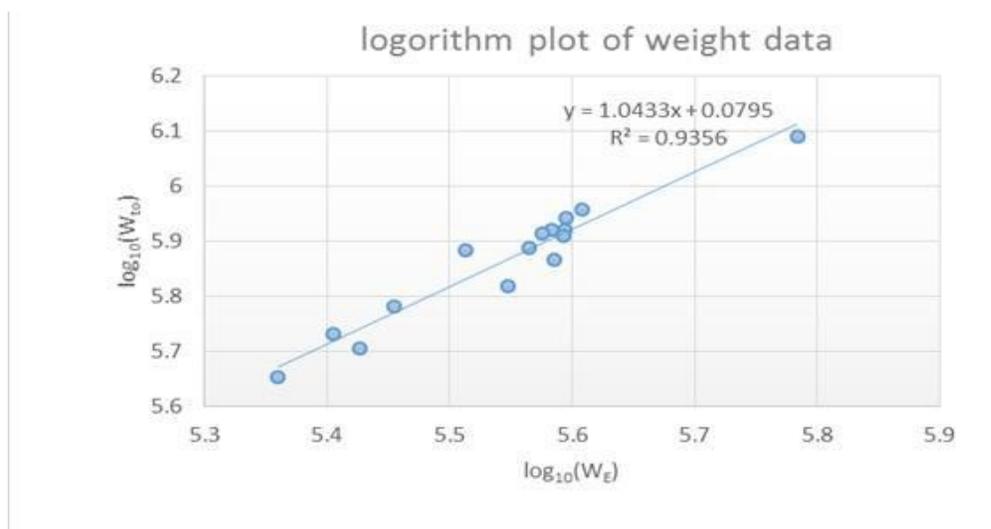
Figure 11: Log-log plot for weight data

3.3 Comparison of Calculated Regression Coefficient with Roskam Data

The estimated values of regression coefficient by Roskam and calculated values are shown in table 12. Calculated values are very close to Roskam data. Therefore, for further calculations, calculated value of regression coefficients will be used.

Table 12: Comparison of calculated regression coefficient with Roskam data

Regression Coefficient	Calculated Value	Value according to Roskam
A	0.0795	0.0833
B	1.0433	1.0383

3.4 Manual Calculation of Mission Weights

For initial estimation of weights, reference [24] is used. There is no practical data available for BWB configuration and method used in Reference [24] is for conventional airplane, therefore, some additional assumptions are made to get best initial estimation.

Assumptions:

(A). For cruise lift to drag ratio $\left(\underline{\quad} \right) = 25$

(B). For loiter ($\underline{\quad}$) $= 24.5$

These assumptions are made on the basis of reference [2], which claims that L/D ratio of BWB is 50% higher than conventional configuration.

Procedure for estimating weights:

Step 1. The mission payload weight was assumed as 126000 lbs.

Step 2. For initial guessing of mission TOW benchmarking was done with Boeing 747 8I and it was assumed the blended body would result in 20% weight saving. Therefore $W_{\text{TO-Guess}}$ = 789600 lbs.

Step 3. It consists of calculating mission fuel weight. For this, weight fraction of each stage of mission profile is estimated and then all fractions are multiplied to get total fuel fraction of mission. Mission profile stages and their estimated fuel fractions are listed in table 13.

Table 13: Estimated fuel fraction for each stage

Stage name	Begin weight and end weight	Weight fraction	Equation used or Reference
Stage 1 -Engine start and warm up	W_{TO} ,W_1	W_1/W_{TO}=0. 990	Reference[24]
Stage 2- Taxi	W_1 ,W_2	W_2/W_1=0.990	Reference[24]
Stage 3- Take-off	W_2 , W_3	W_3/W_2=0.995	Reference[24]
Stage 4- Climb to cruise altitude and accelerate to cruise speed	W_3 , W_4	W_4/W_3=0.90	Reference[24]
Stage 5 - Cruise	W_4 ,W_5	W_5/W_4=0.741	$= ($ ___ $)$ (___) ___ (1) Where, $= 0.5$ h) , RCR= 9712 miles, Assumption (___) = 25
Stage 6- Loiter	W_5 , W_6	W_6/W_5=0.992	$= ($ ___ $)$ (___) ___ (2) $= 0.6$ Assumption (___) = 24.5 and E_{LTR}= 0.33 hrs.
Stage 7 - Descent	W_6 ,W_7	W_7/W_6=0.990	Reference[24]
Stage 8 - Flying to the alternate airport.	W_7 ,W_8	W_8/W_7=0.990	Reference[24]

Stage 9 - Landing, taxi and shut down	W_8 , W_9	$W_9/W_8=0.992$	Reference[24]	

Total mission used fuel fraction W_{FF} is given by:

$$W_{FF}=(\underline{\quad 1 \quad})(\underline{\quad 2 \quad})(\underline{\quad 3 \quad})(\underline{\quad 4 \quad})(\underline{\quad 5 \quad})(\underline{\quad 6 \quad})(\underline{\quad 7 \quad})(\underline{\quad 8 \quad})(\underline{\quad 9 \quad})=0.634 \tag{3}$$

$$\underline{\quad} = (1 - \quad) = 289783.2 \text{ lbs.}$$

Weight of mission fuel (W_F) = weight of fuel used +weight of trapped fuel

$$W_F= 292625.76 \text{ lbs.}$$

Step 4. $W_{E\text{-tent}} = W_{TO\text{-guess}} - W_F - W_{PL}$ $\tag{4}$

$$W_{E\text{-tent}} = 789600 – 292625.7 - 123060 = 372369 \text{ lbs.}$$

Step 6. To find $W_{E\text{-allow}}$, the following equation was used:

$$W_{E\text{-allow}} = \text{invlog}_{10} [(\log_{10} W_{TO} -- A) / B] \tag{5}$$

Where the regression coefficients A and B were found to be 0.0795 and 1.0433.

$$W_{E\text{-allow}}= 377091 \text{ lbs.}$$

Step 7. The $W_{E\text{-tent}}$ and $W_{E\text{-allow}}$ are not within the 0.5% tolerance, therefore further iterations are needed. After iterations, Final weight: $W_{TO}= 823767$ lbs., $W_E= 392718$ lbs.

3.5 Calculation of Mission Weights using the AAA Program
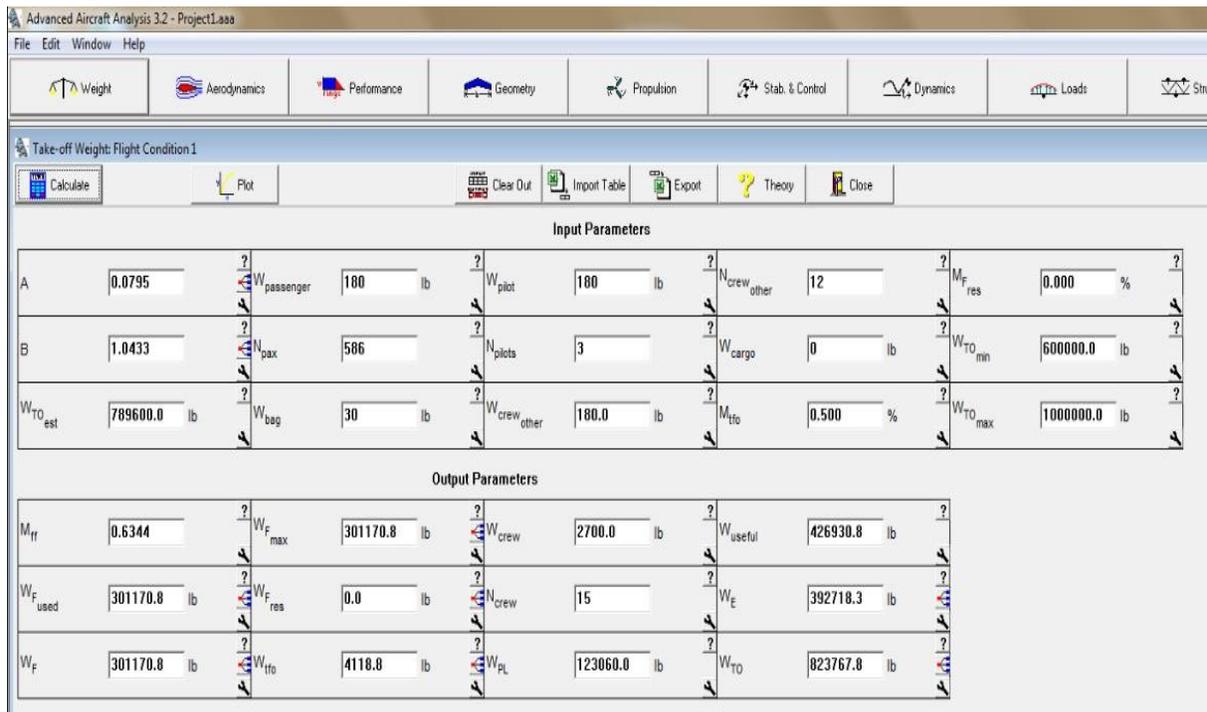
Figure 12: Calculation of Mission Weights using the AAA Program
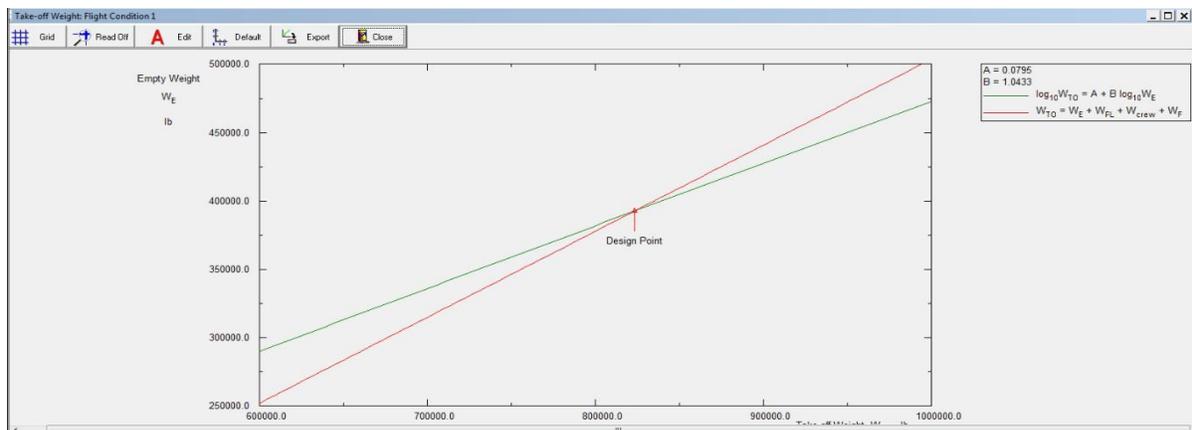
Figure 13: Weight design point

3.6 Takeoff Weight Sensitivities

It is important to conduct weight sensitivities analysis in order to find which parameters

drive the design and which areas of technological change to be pursued in case new mission

capability must be achieved. For takeoff weight sensitivities, calculations reference [24] is used.

3.6.1 For the Sensitivity of Take-off Weight to Payload Weight

$$\underline{\quad} = \quad (\ -\ (1\ -\ )\ )^{-1} \tag{6}$$

Where, A and B were calculated in section. C and D are calculated using the following equation

$$= \{1\ -\ (1\ -)(1\ -\ )\ -) \tag{7}$$

$$= \tag{8}$$

Here, M_{tfo} can be assumed to be zero and M_{res}=.10, from the calculations, C=0.670 and D= 123060

$$= 5.83$$

The factor 5.83 is the growth factor due to payload for BWB 600 aircraft. This means that for each pound increase in payload weight, the gross take-off weight will have to be increased by 5.83 lbs.

3.6.2 For Sensitivity of Take-off Weight to Empty Weight

$$\underline{\quad} = \quad [\quad \{\underline{\quad 10-\quad}\}]^{-1} \tag{9}$$

$$= 2.19$$

The factor 2.19 is the growth factor due to empty weight for BWB 600 aircraft. This means that for each pound increase in empty weight, the gross take-off weight will have to be increased by 2.19 lbs.

3.6.3 For Sensitivity of Take-off Weight to Range

$$-1 \tag{10}$$

$$F = -BW_{TO}^{2}\{CW_{TO}(1 - B) - D\}^{-1}(1 + M_{res})M_{ff} \tag{11}$$

F=3361834.85 lbs.

$$= 124.5 \; /$$

The factor 124.5 is the growth factor per unit range for BWB 600 aircraft. This means that for each mile increase in range, the gross take-off weight will have to be increased by 124.5 lbs.

Table 14: Weight sensitivity table

$\dfrac{\partial W_{TO}}{\partial W_{PL}}$	5.83
$\dfrac{\partial W_{TO}}{\partial W_E}$	2.19
$\dfrac{\partial W_{TO}}{\partial R}$	124.5 lbs/miles

4.0 Performance Sizing

The aircraft is sized according to FAR 25 requirements. The design point is obtained from the

performance graph plotted according to reference [24].
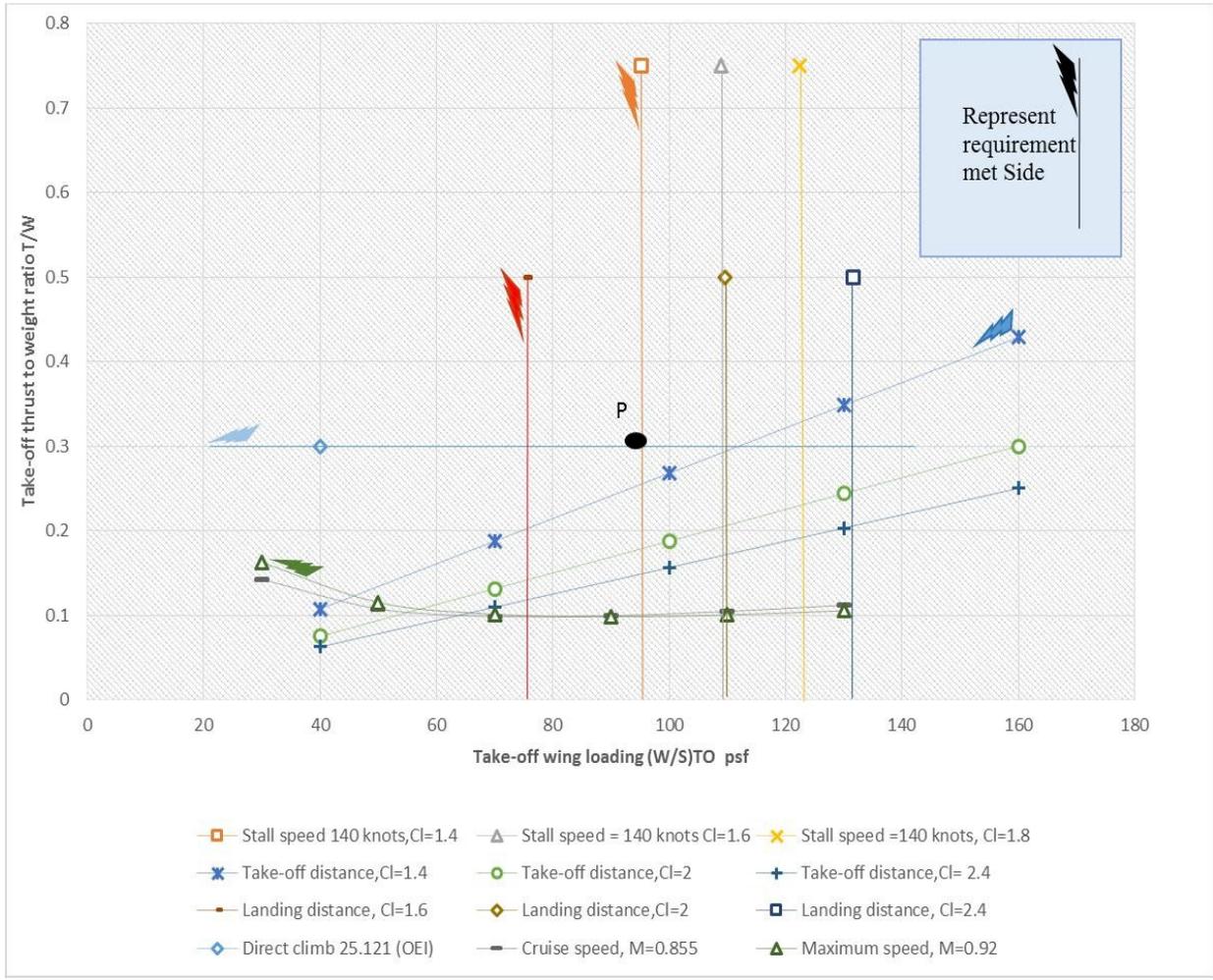
Figure 14: Performance sizing chart

4.1 Summary of Performance Sizing

The design point chosen is shown as point P on the sizing graph. The table shows the initial

specifications of BWB 601 according to design point.

Table 15: Summary of performance sizing

Take-off wing loading (lbs./ft^2)	92
Aspect ratio	6
Stall speed (knots)	140
Wetted area (ft^2)	31471
Wing area (ft^2)	9601
Take-off thrust (lbf)	264,990
Maximum take-of lift coefficient required with flaps up (clean) C_{Lmax}	1.6
Maximum lift coefficient required for landing C_{Lmax-l}	2

5.0 Center body and Wing design

5.1 Airfoil Selection

The selection of airfoil is very important aspect of design. While high lift and low drag coefficients are the requirements of performance, the moment coefficient (C_m) plays a role in stability behavior of an airplane: it affects the longitudinal stability. In conventional airplane, airfoil is designed for negative moment coefficient, which is compensated by the horizontal tail to stabilize longitudinally. Tailless aircraft obviously can't compensate for negative moment as they don't have horizontal tail. Longitudinal stability of tailless aircraft can be obtained in two ways: using reflex airfoil or by using Sweep and twist wings [12]. How these two designs incorporate stability will be discussed in detail in stability section of this report.

In case of swept back wing, any airfoil can be used by selecting a suitable combination of sweep and twist [12]. Longitudinal stability is provided by combination of sweep and twist. In order to get good performance, it is best to choose airfoil with very low pitching moments. The low pitching moment airfoil thus will require smaller amount of twist which results in a broader speed range without paying too much penalties off the design point.

Both, increasing reflex in camber line and twist in swept wing affect the performance, so it is desired to select airfoil which is best suited for required mission. Keeping performance in mind, it was decided to use reflex airfoil for center body and cambered airfoil for outboard and tip. Stability for airplane will be achieved through combination of center body airfoil (reflex) and wing twists, whereas high lift and 'high lift to drag ratio' will be achieved from outboard cambered airfoil.

5.1.1 Center Body (Inboard) Airfoil

The airfoil chosen for center body should have medium thickness, large leading edge radius, high stall angle, possible high lift to drag ratio along with positive pitching moment coefficient. Java foil software, which is interactive database and program, was used to analyze different airfoils listed in table 15. The present conceptual design work selected NACA 23112 (Reflex) as the most suitable for the center body of BWB601. Shape and Polar plots for NACA 23112 generated by using 'Java foil' are shown in Fig 15 and Fig 16.

Table 16: Comparison of different airfoils for center body

	Lie back LA2573 A	NACA 23112	Eppler 635	MH-62	MH-60
Max Camber	3.2% at 26.1% C	1.2% at 14.7% C	2.889	1.5% at 37.4% C	1.8% at 38.10%C
Max Thickness	13.7%	12%	11.616	9.30%	10.28%
$C_{l\text{-}max}$	1.3	1.55	0.964	1.2	0.906
$C_{m\text{-}c/4}$	0.02	0.03	.04	-0.004	+0.0175
$(L/D)_{max}$	18.549	42.28	22.883	67.897	65.726
Stall angle	12	13	14	8.0	9.0
Angle of attack for Max L/D	10.5	4.5	4	6.5	6.0
Zero lift angle	0.0	-0.5	0.5	-0.5	0.0
Lower flatness	56.1	72.1 %	64.6%	68.3%	65.0%
Leading edge radius	3.2	3.8 %	2.1 %	0.6 %	0.6
Trailing edge angle	7.0	14.40	13.4	4.3	4.6
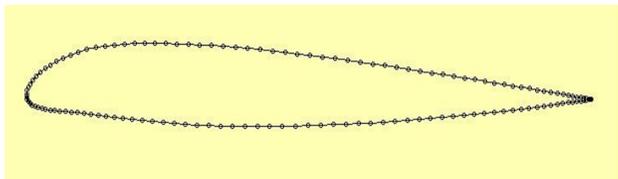
Figure 15: Airfoil for Center body (NACA 23112)
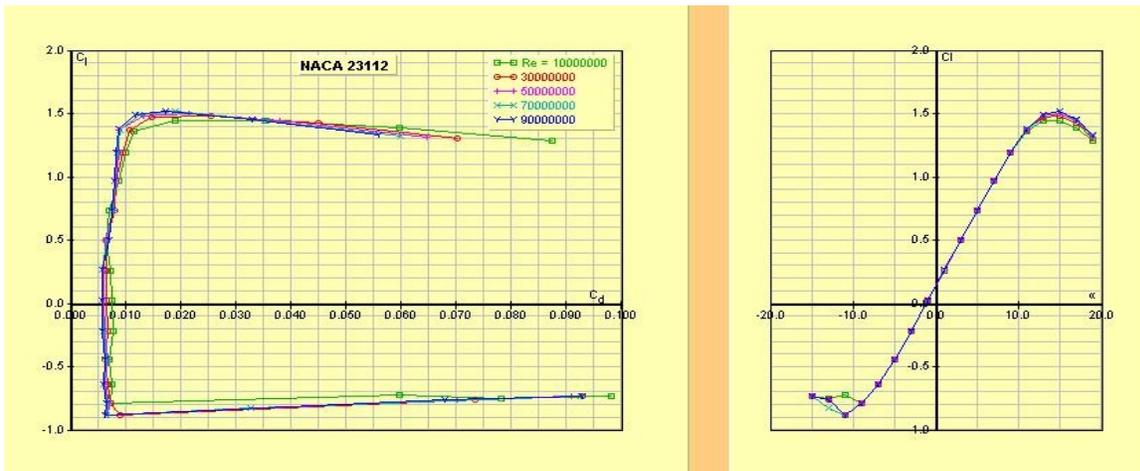
Figure 16: Polar plots for NACA 23112 (Reflex) Airfoil.

5.1.2 Outboard and Tip Airfoil

The outboard airfoil is crucial part of aircraft design as majority of the lift will be generated by this section. Also, the region in between outboard and Tip will be holding fuel and main landing gear, therefore it must be of considerable thickness. So, outboard and tip airfoil should have high lift to drag ratio, high lift, high thickness and good stall characteristics. Number of candidate airfoils (as listed in table 17) were studied and compared to select the best airfoil. From the comparison the FX 60-126 airfoil was selected for outboard and tip sections of wing. Shape and Polar plots of FX 60-126 airfoil generated by using 'Java foil' are shown in Fig 17 and Fig 18.

Table 17: Comparison of different airfoils for outboard and tip

	FX60-126	GOE 440	Eppler 395	FX 61-140	MH 115
Max Camber	3.6%	9.7%	5.3	2.5%	5.6%

Max Thickness	12.6%	15.2%	12.3	14%	11.1
Cl_{max}	1.491	1.864	1.589	1.422	1.725
$(L/D)_{max}$	145.5	117.308	106.8	105.93	107.008
Stall angle	10	0.5^0	8.0	6.5	7.0
Angle of attack for Max L/D	5	2.5^0	5	5.5	4.5
Zero lift angle	-4.5	-11.5^0	-6.5	-5.0	-6.5
Lower flatness	52.8%	74.8%	69.9	27.8	84.7%
Leading edge radius	2.6	3.2%	0.8	1.2%	1.6
Trailing edge angle	2.6	9.5	7.4	6.3	7.2
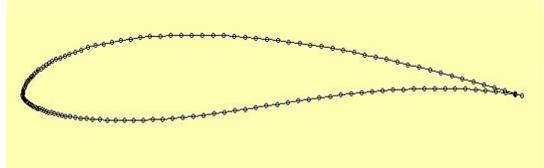
Figure 17: Airfoil for Outboard and tip Airfoil (FX -60126)
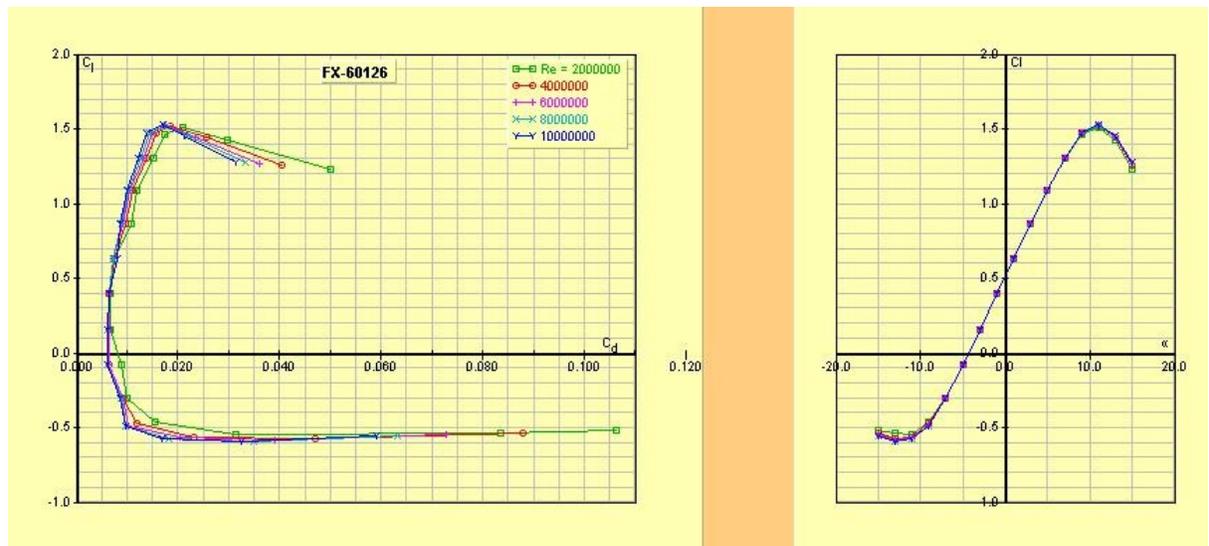
Figure 18: Polar plots for FX-60126 Airfoil.

5.2 Center Body Design

In Blended Wing Body configuration, both the fuselage (center body) and wings are integrated with each other smoothly and acts as a single body. The center body is composed of distinct and separate wing structures, though the wings are smoothly blended into it.

The center body or fuselage results in most of the drag of the airplane (25-50 percent), therefore center body of aircraft is designed in a shape to have minimum possible drag. Various drags which act on fuselage are [6]:

(A).   Friction drag

(B).   Profile drag

(C).   Base drag

(D).   Compressibility drag or wave drag

(E).   Induced drag

In order to have minimum friction drag, minimum wetted area is required for a given volume, which further depends upon the shape of the body. Effect of shape on wetted area can be observed in Fig 19. Sphere is the best option for minimum friction drag but it's not conducive to the streamlines and thus increases drag. Flatted disc is the second best option for minimum friction drag [14]. Profile and base drag is determined by the front and after body shape. To have minimum profile and base drag, ideal streamline flow is required over nose and tail. The drag related with compressibility due to high speed is called compressibility drag. The compressibility drag includes any variation of the viscous and vortex drag with Mach number, shock-wave drag, and any drag due to shock-induced separations. Compressibility drag can be reduced by increasing sweep angle.

Cylinder shape used in conventional airplanes has lesser frontal area that results in lesser profile and base drag as compared to BWB configuration. But cylindrical fuselage has more frictional drag due to more wetted area than BWB fuselage for same volume

During designing of fuselage, trade-off has to be made between various drags to get best possible shape. For BWB 601 fuselage, sphere is flattened to streamlined disk, which is integrated with wings to have minimum wetted area.
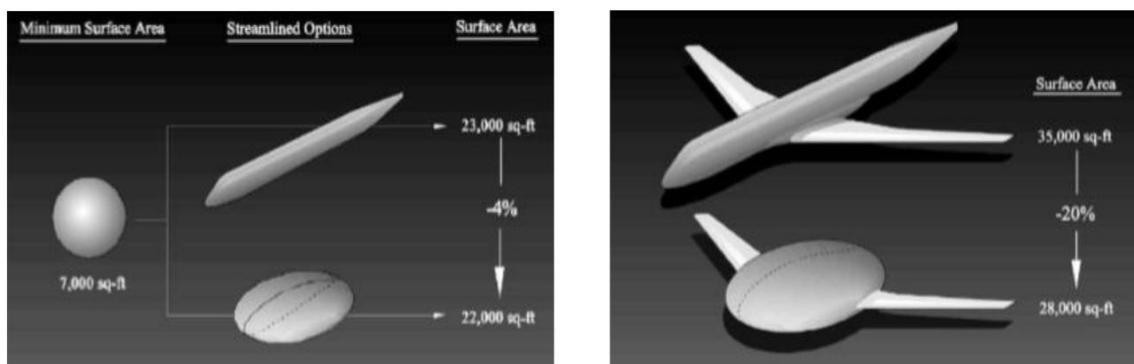
Figure 19: Effect of shape on wetted area [14]

The cabin has to be designed for internal pressure in addition to bending, shear and torsional loads. It should be noted that disc shape cabin requires more strength for same internal pressure as compared to conventional cylindrical; this is due to the fact that in a conventional cylindrical fuselage, internal pressures are carried more efficiently in hoop stresses by a thin skin, whereas for disc shape fuselage, internal pressure induces large bending stresses which require heavier structure. Studies have been conducted by NASA and Boeing to address this structural issue [4]. They investigated two concepts: Multi bubble fuselage structure and single strong shell (Fig 20 and Fig 21). Multi bubble structure consisted of cylindrical shells inside main disc for sustain internal pressure loads and outer skin to support bending. Boeing argued with multi-bubble theory and raised the issue that outer skin still needs to be designed to take internal pressure loads in case there is any leakage in the inner bubble. As the outer skin has to be designed for internal

pressure, there is no point to build inner shells. Their research concluded to use single shell structure strong enough able to withstands all the loads. The additional weight due to heavy structure should not be problem as the aerodynamic gains from BWB configuration will outnumber this weight increase. For BWB 601 cabin design, single shell approach will be used (Fig 21).
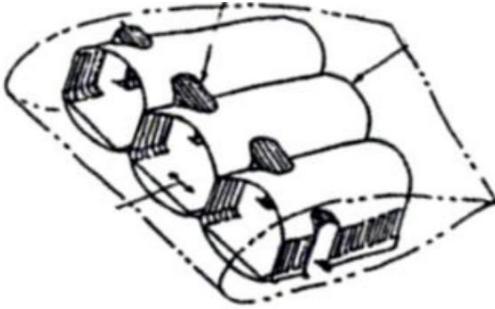
Figure 20: Multi bubble structure [4]
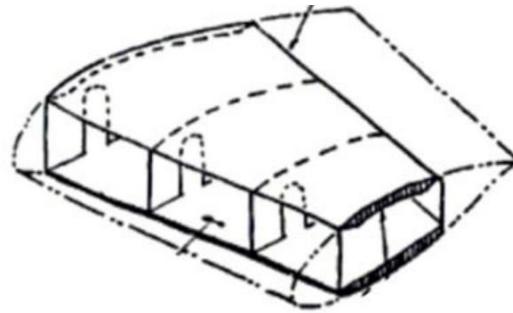
Figure 21: Integrated skin and shell [4]

Overall structural configuration of BWB will be swept back wing body. A swept back wing offers the advantage of delaying drag rise caused by compressibility near sonic speeds, so they are favored for high subsonic and supersonic speeds. Center body has the maximum thickness that will cause high drag, therefore needs higher sweep than outboard wing.

5.2.1 Cabin Layout

For passenger aircraft, design of cabin layout must meet FAR 25 requirements. The fuselage of BWB 601 is required to enclose a space for total number of 601 people (including flight attendants) plus galleries, lavatories and space for baggage. Size of cross section is mainly affected by number of seats abreast. Higher abreast seating capacity provides the opportunity for extension in coming models and thus shorter the fuselage, easier it becomes to grow plane in future. The BWB body gives the advantage of higher abreast seating. Cabin layout is designed according

to reference [24]. The cabin is designed for 28 First class, 86 business class and 472 economy class seats. The dimensions of seats for these three categories are listed below in table 18. Space for 18 galleries and 25 lavatories is provided considering the large number of passengers.

Table 18: Seat Dimensions

Seat	Width	Seat Pitch	Aisle Width
First class	25	40	23
Business class	23	36	21
Economy class	21	32	20

Figure 22: AutoCAD drawing of Cabin Layout

5.3 Wing Design

This section deals with some of the considerations involved in wing design, including the selection of basic sizing parameters and more detailed design. Wing is the most important aspect of aircraft design, which decides how well the airplane will fly. Wing design or shape depends upon the mission requirements: type of aircraft, performance, speed, operating altitudes, gross weight, and space requirements for engine and fuel tanks. Depending upon mission requirements, wing configuration can be selected from following:

a) Rectangular configuration

b) Elliptical configuration

c) Swept wing configuration

d) Delta wings configuration

While each configuration works well, they all have certain restrictions and limitations making them suitable only for certain requirements. The swept wing is the "way to go" for jet powered aircraft. It needs more forward speed to produce lift than the rectangular wing, but results in much less drag in the process, meaning that the aircraft can fly fast with higher efficiency. It also works well at the higher altitudes, which is where most jet aircraft fly [20].

There are essentially two approaches to wing design [34]. In the direct approach, one finds the planform and twist that minimize some combination of structural weight, drag, and C_{L-max} constraints. The indirect approach involves selecting a desirable lift distribution and then computing the twist, taper, and thickness distributions that are required to achieve this distribution. The latter approach is generally used in preliminary design to obtain analytic solutions and insight into the important aspects of the design problem, but is difficult to incorporate certain constraints and off-design considerations in this approach. The direct method, often used in the latter stages of wing design for depth investigation on preliminary selected parameters. In this report, indirect approach is used to design a wing.

Wing lift and load distributions play a key role in wing design. Main objective of wing design is to generate the lift such that the span wise lift distribution is elliptical [34]. Elliptical lift distribution ensures lower induced drag, lighter wing structure, better control and stall characteristics. From performance sizing section, wing surface area and aspect ratio were calculated as 9601 ft^2 and 6 respectively. Wing span can be calculated from equation

$$= \quad \frac{}{\quad}^{2} \quad \rightarrow b= 240 \text{ ft} \tag{12}$$

In blended body case, the wing and fuselage (center body) act as single lifting surface. The center body is referred to as inboard wing and the outer body is referred to as outboard wing in this report. Both Inboard and outboard wing parameters are driven by different requirements and must met their individual needs. Inboard need to be thicker than outer one to meet the volume requirements of cabin.

5.3.1 Inboard wing

Inboard wing design is designed to carry payload load as well to generate lift. Most of the dimensions are decided by the cabin volume requirement. Wing thickness ratio is decided by airfoil used, $=$ 12 from center body airfoil selection. For BWB, the center body frontal area is large so

high drag is expected unless high sweep is provided to wing. Also high thickness ratio would result in low critical Mach number i.e. early rise of drag. To increase the critical Mach number, design requires high wing sweep. Figure 23, depicts the effect of thickness ratio and sweep angle on critical Mach number. For initial design, sweep angle 60 degree is chosen to avoid early rise of drag.
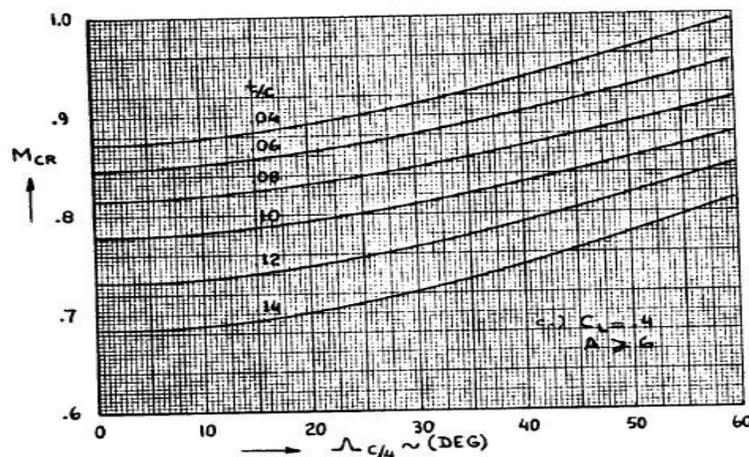
Figure 23: Effect of thickness ratio and sweep angle on critical Mach number [24]

Taper ratio is calculated as

$$1 = \frac{36.1}{117.8} = 0.306 \tag{13}$$

Calculations of inboard wing characteristics and parameters:

(A). Inboard wing area S_1= Area under Fig 22= 4813 ft^2

(B). From airfoil (NACA 23112) characteristics $C_{l\text{-max}}$ =1.555

(C). $$\overline{} = \frac{-0.4}{} \qquad [24] \tag{14}$$

Where, W take-off weight of airplane in newton, W_F is mission fuel weight, q_∞ is free stream dynamic pressure at 43000 ft.

$$= \frac{1}{2}\rho \quad ^2 \tag{15}$$

$\rho = 0.262$ kg/m^3

Using equations (14) and (15), we get

(D). $$\overline{} = \frac{.319}{^2} \qquad [37] \tag{16}$$

$$= ^{-1}(\quad \underline{} \quad) \tag{17}$$

Where, V_c is the vertical components of velocity during climb.
From equations (16) and (17), we get $\underline{} = 0.807$

(E) To figure out the twist Stanford Java Wing analysis program is used [27]. This program uses discrete vortex Weissinger computations to calculate and plot the lift & coefficient of lift distributions, and also displays efficiency & induced drag coefficients. Twist angle was varied to get lift distribution close to elliptical distribution (e=1). From this trade study twist angle ($_1$) = 0 degree.

5.3.2 Outboard wing

Calculations of outboard wing characteristics and parameters:

(A).   Outboard wing area, $S_2 = S - S_1 = 4798$ ft^2.

(B).   Wing span for outboard wing $b_2 = b - b_1 = 240 - 76 = 164$ ft.

Aspect ratio for outboard wing can be calculated as

(C).   Using equations (14) and (15), we get $\quad = .320$

(D).

(E).   Using equations (16) and (17), we get $\quad = 0.809$

(F)   From airfoil (FX -60126), $C_{l\text{-max}} = 1.499$

Again, Stanford Java Wing analysis program is used [27] to find out twist in wing. Sweep angle and twist angle were varied to get lift distribution close to elliptical distribution (e=1). From this trade study twist angle ($_1$) = 4 degree.

Table 19: Selected configuration for outboard and inboard wing

	C_{Lmax}	Stall angle	Taper ( )	Sweep angle Λ (degree)	Twist angle ϕ (degree)	e	Dihedral angle
Outboard wing	1.44	18.5	0.5	30	4	0.995	3
Inboard wing	1.27	27.5	0.302	60	0	0.987	0

5.3.3 Drawings of wing general layout.

All dimensions in inches.
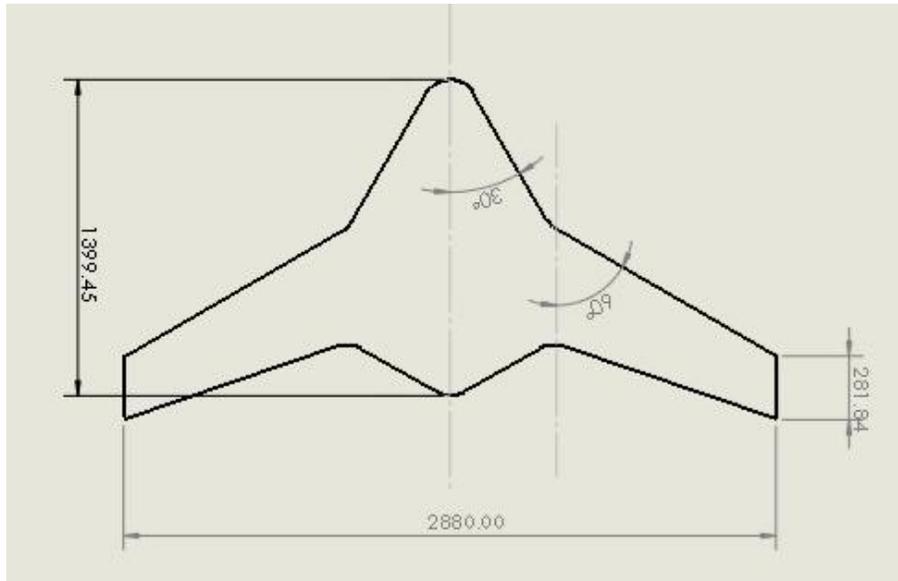
Figure 24: Top view of wing (Solid work drawing)
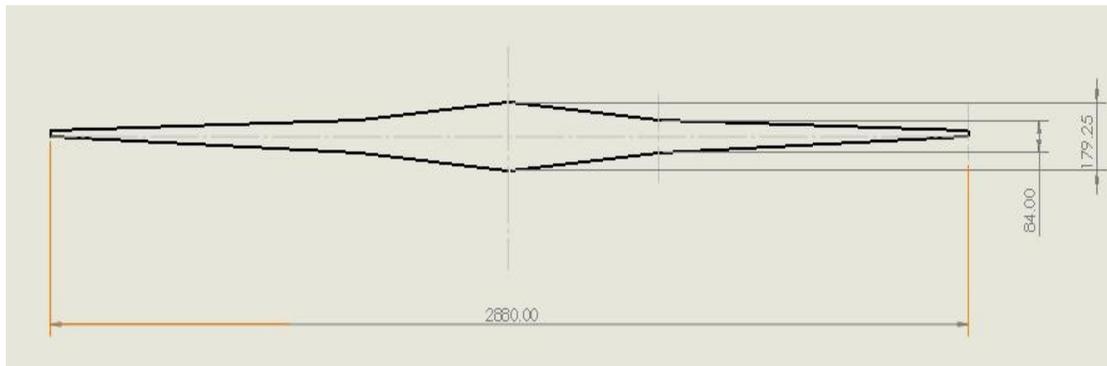
Figure 25: Front view wing (Solid work drawing)

6.0 Selection and Integration of Propulsion System

6.1 Propulsion system selection

Type of propulsion system used in an airplane depends upon the mission requirements and other factors like cost, reliability, maintainability and timely certification. Turbofan type engine was selected after comparing the mission profile of BWB 601 with Fig 32 [24].

In order to avoid complexity of development and certification of engine, it was decided to select engine that is already existent in market. Trade study was done between the different engines listed in table 20 to pick engine for BWM 601.
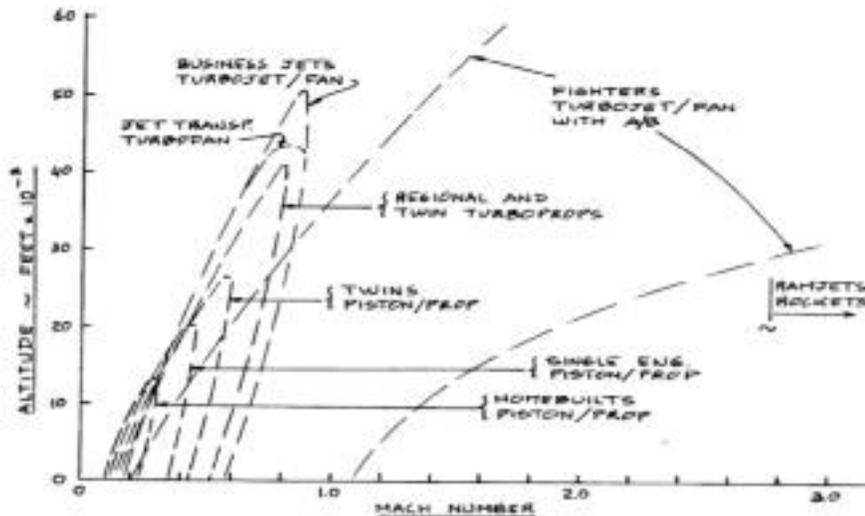
Figure 26: Engine type used in relation to speed altitude envelope of airplane [6]

Table 20: Comparison of some of the world's powerful jet engines [8] [10]

	GEnx-2B67 (B747-8)	GEnx-1B70 (B787)	Trent 900	GE 90-115 B
Takeoff thrust (lbs)	67000	69800	75,000–84,000	115000
Bypass ratio	8.0	9.1	8.5-8.7	
Overall pressure ratio	44.7	43.5	37-39	42
Air Mass flow (lbs./sec)	2297	2545		

Fan Diameter (inch)	104.7	111.1	155.3	126.7
Bare engine length (inch)	169.7	184.7	215	287
Compressor stages (Fan/booster/HPC)	1/3/10	1/4/10	1/8/6	1/4/9
Turbine stages (HP/LP)	2/6	2/7	1/5	2/6
Thrust to weight ratio		5.64	5.46-6.11	6.3
Dry weight (lbs.)	12400	12822	13770	18260

Out of the engines listed in table 20, Genx-2B67 and Trent 900 are well proven engines for large transport aircraft and they are being used in Boeing 747-8I and Airbus A380 respectively. Although both these engines are very efficient and reliable, but for the required mission, aircraft Genx-2B67 has more to offer than Rolls Royce's Trent 900. Genx-2B67 is smaller in size and is lighter in weight compared to Trent 900, which gives advantages like less drag and more aerodynamic efficiency. The Genx-2B67 produced by GE aviation uses latest generation materials and design processes to reduce weight, improve performance and requires less maintenance [30]. BWB 601 requires 264,990 lbf of takeoff thrust; therefore, four Genx-2B67 (4x67000) engines will be used. The selected engine meets all the mission requirements along with low fuel burn and excellent environmental attributes.

Figure 27: Genx-2B67 [11].

6.2 Disposition of Engines or Integration

The engine will be placed on the top of center body at aft location, to offer noise shielding. There are two options for aft engine mounting: First one is, simply mounting the engines on pylons, but for this, penalty of increased wetted area, weight and ram drag has to be paid. Second option is to mount engine directly on the upper surface and take the advantage of ingestion of the boundary layer generated. In principle, boundary layer ingestion can improve the propulsive efficiency by reducing ram drag. This assumes that an inlet can be designed such that it provides proper pressure recovery and uniform flow at the fan face of the engine.

Studies on the boundary layer ingestion concept were conducted at the University of Southern California and at Stanford University [29]. Results showed that proper configurations of vortex generators could provide a reasonably uniform flow at the fan face with acceptable pressure recovery. Although boundary layer concept requires further investigation to validate it for practical application, but in this report, it is assumed that results will hold good for practical aircraft. Therefore, three-engine configuration with upper surface boundary layer ingestion inlets and S-ducts to the engines is selected.

7.0 Landing Gear Design

A retractable two twin tri-tandem main landing gear is chosen to provide enough strength required during landing and take-off of large passenger aircraft. The design of landing gear depends on tip over criteria and ground clearance criteria [24]. To provide adequate ground clearance, the length of nose gear is chosen as 11 ft and for middle & rear tandem landing gear as 10 ft.

The nose gear is located at 10 ft, center tandem at 68.3 ft and rear tandem at 95 ft from nose respectively. The maximum static load per strut for main gear (Pm) and nose gear (Pn) can be calculated from following equations as [24]:

$$\rule{2cm}{0.4pt} \quad = 0.94 \tag{22}$$

$$\rule{1.5cm}{0.4pt} \quad = 0.06 \tag{23}$$

Where, W_{TO} is gross takeoff weight and n=4 is the number of main gear struts. By using equation (22), (23) and typical landing gear data [24], other specifications can be easily obtained. AutoCAD drawing of general layout is shown in Fig 34.
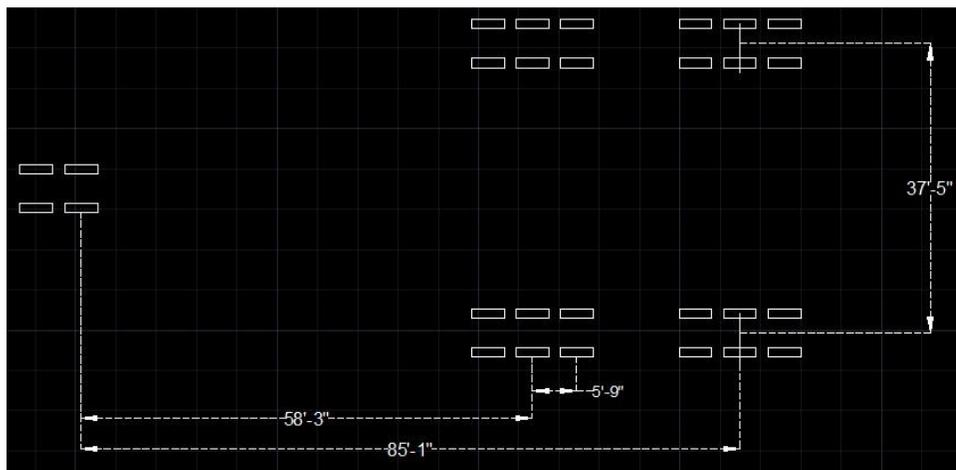

Figure 28: AutoCAD drawing of Landing Gear layout

8.0 Longitudinal Static stability

8.1 Basic requirement of longitudinal static stability

Static stability describes the aircraft's initial response to a disturbance. If the aircraft has tendency to return back to equilibrium after a disturbance, then it is called positive static stable and if it continues in perturbed state, then it is called neutrally stable and if it moves further away from equilibrium state, then it is called negative static stable aircraft.

Longitudinal stability means ability of aircraft to recover from an angle of attack disturbance. This quality of aircraft is also called pitch stiffness and is defined as change in pitching moment coefficient for a given change in angle of attack. For the aircraft to be statically stable in pitch, the variation in pitching moment with alpha must be negative. Therefore an increase in angle of attack will generate a negative pitching moment about the CG, bringing the aircraft back to its trim condition. Therefore, for aircraft to be stable, < 0.

Now consider two airplanes A and B as shown in the Fig 35. Both aircraft have positive static stability i.e. < 0. The slope line of aircraft A intersects the x axis at positive angle of

attack whereas slope line of aircraft B intersects x axis at negative angle of attack. This means that aircraft A can be trimmed at positive angle of attack whereas aircraft B cannot be trimmed at positive angle of attack. In other words, in order to trim aircraft at positive angle of attack, it is required to have $_0 > 0$. To sum up, following two conditions must be met for positive pitch stability:

$$< 0 \tag{24}$$

$$_0 \quad > 0 \tag{25}$$
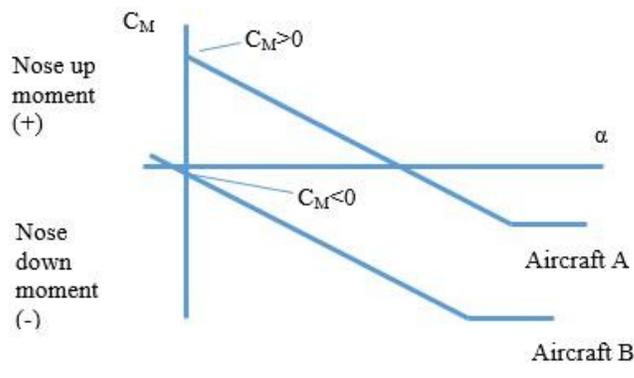
Figure 29: Moment slope of aircraft A and aircraft B

Consider wing and tail configuration as shown in Fig 36. For this analysis, the moments generated by fuselage, propulsion system and drag on tail have been neglected. It is also assumed that angle of attack is small such that cos α=1
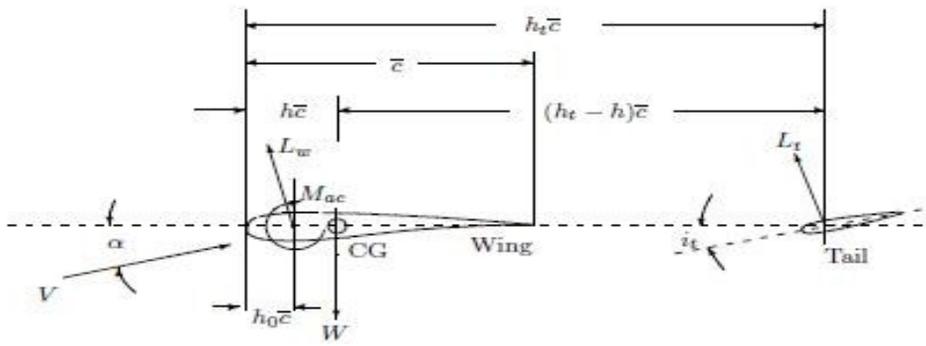
Figure 30: Free body diagram of conventional tail wing configuration [10]

$$= + (h - h_0)\Gamma - (h - h)\Gamma \tag{26}$$

Non- dimensionalzing the above equation by dividing with $\overline{\ }$,

$$= + (h - h) - (h - h) \underline{\ } \tag{27}$$

Assuming linear varition of tail lift coefficent , can be defined as

$$= [(1 - \varepsilon /) -] \tag{28}$$

Also wing lift coefficient can be expressed as linear relationship, $=$ Therefore,

$$= \quad + (h - h_0) \quad - (h - h) \quad [\quad (1 - \frac{\varepsilon}{}) - \quad]$$

For α=0,

$\overline{\qquad}$

to α, $\qquad _0 = + (h - h)$ Differentiating with respect

(29)

(30)

$$= (h - h) \qquad - (h - h)\underline{\qquad} \qquad (1 - \frac{\varepsilon}{})$$

(31)

$_\circ$

$- _{\circ^+}$

(32)

From equation 25, we argued that for positive pitch stability $_0 > 0$. Examining equation 30, it can be seen that for a tailed aircraft, $_0$ has two parts: first part due to wing and second

part due to fixed incidence of tail. To take aerodynamic advantage, most aircraft use positive camber airfoil which results in negative pitching moment < 0. Therefore overall $_0$ is then

made positive by second term of the equation. So, most designs include horizontal tail to counteract negative pitching moment of wing and provide overall positive moment. Horizontal tails are placed at negative incidence so as to lift down the aircraft at rear end and pitch the nose up.

8.2 Stability for Blended wing body without tail

For Blended wing body aircraft without tail, equation 30 reduces to:

$$_0 =$$

(33)

So, tailless aircraft obviously can't compensate for negative moment. In order to provide longitudinally stability to tailless aircraft, any of the following two designs can be incorporated [12]:

A) By use of combination of sweep and twist

In case of swept back wings, any airfoil can be used by selecting a suitable combination of sweep and twist (Fig 38). Longitudinal stability is provided by combination of sweep and twist. To obtain positive $_0$ in wing only configuration, the wash out is provided i.e. wings are twisted so that angle of incidence is lower at tips. Negative moment generated by root airfoil is compensated by generating positive moment from wing tips. Due to twist in wing, negative lift is generated at near wing tips which results in overall positive moment coefficient.
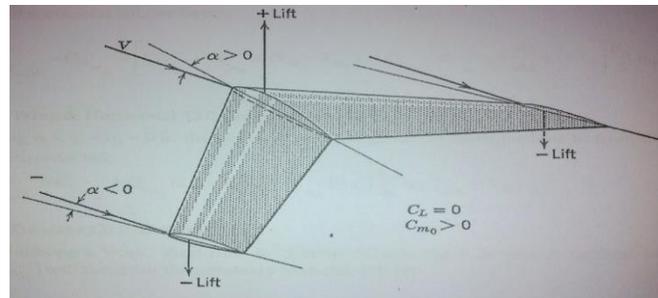
Figure 31: Forces acting on swept back wing [36]

B) By use of Reflex Airfoil

By using a reflex camber airfoil and placing the center of gravity front of quarter chord point, static longitudinal stability can be achieved (Fig 32). Reflex camber line produce positive pitching moment and aerodynamic force will act behind the CG. If aircraft nose is pitched up by disturbance, then lift will increase and with $L_2 > L_1$, it will result in pitch down moment, reducing the angle of attack, until the equilibrium state is reached again. Thus, reflexed airfoil can provide stability to aircraft. Problem with reflex airfoil is that it shifts the lift vs drag polar down, which means lower coefficient of lift at certain angle of attack and also less maximum lift coefficient [12].
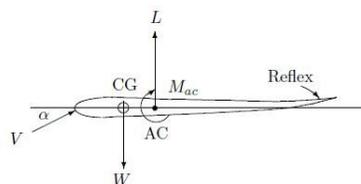
Figure 32: Free body diagram of reflex airfoil [3]

8.2.1 Estimation of neutral point

Neutral point is the reference point for which pitching moment does not depend on the angle of attack. Neutral point only depends upon the plane's external geometry. XFLR 5 software was used to find neutral point. By trial and error, CG was moved backward and polar's for Cm vs alpha were plotted until straight horizontal curve was obtained, which tells the location of neutral point. For straight horizontal curve $X_{NP}=X_{CG}=73$ ft
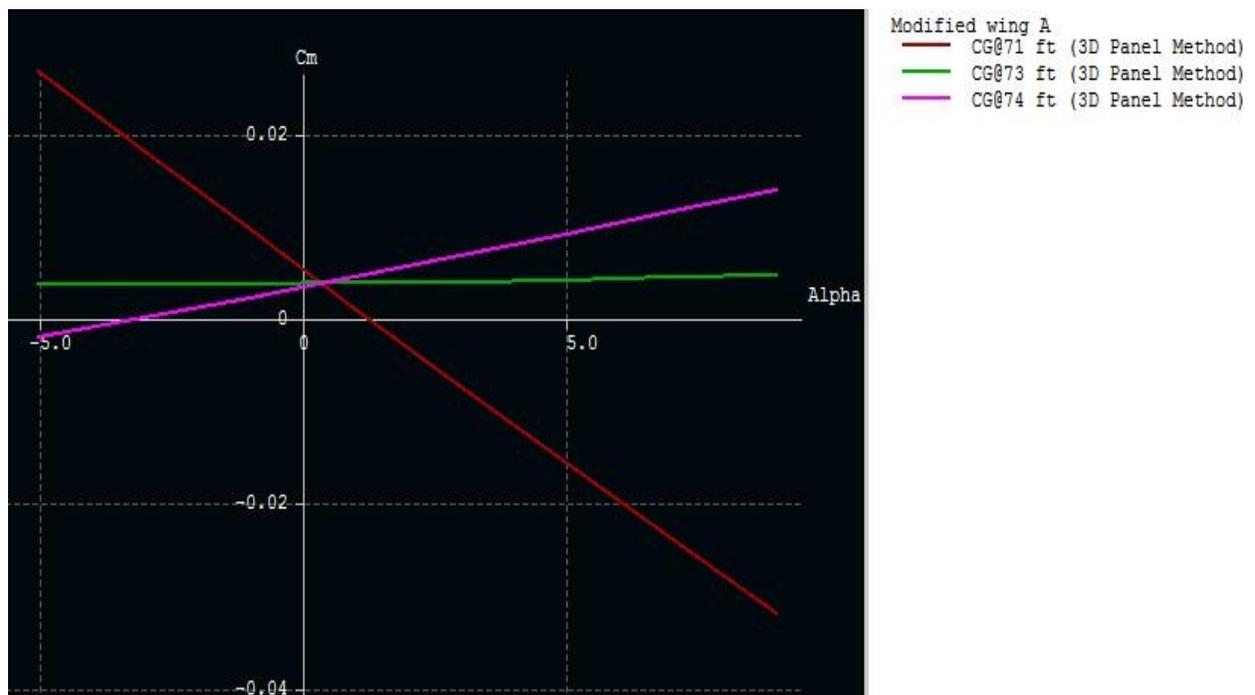
Figure 33: Cm vs alpha graphs for different CG locations

8.2.2 Weight and Balance

Components weight are approximated by using Roskam class I method. For brevity only the main components are considered and there weight's along with their point mass location is presented in table 21.

Table 21: Point masses and their locations

Description	Mass	Location	x (ft)	y (ft)	z (ft)
Fixed equipment's	73,315	A	30.000	0.000	0.000
Landing Gear	46,246	B	73.000	0.000	-2.000
Wing	209,237	C	65.926	0.000	1.520
Payload	123,060	D	75.000	0.000	0.000
Fuel	301,170	E	78.000	0.000	2.000
Propulsion system	61,073	F	105.000	0.000	4.000
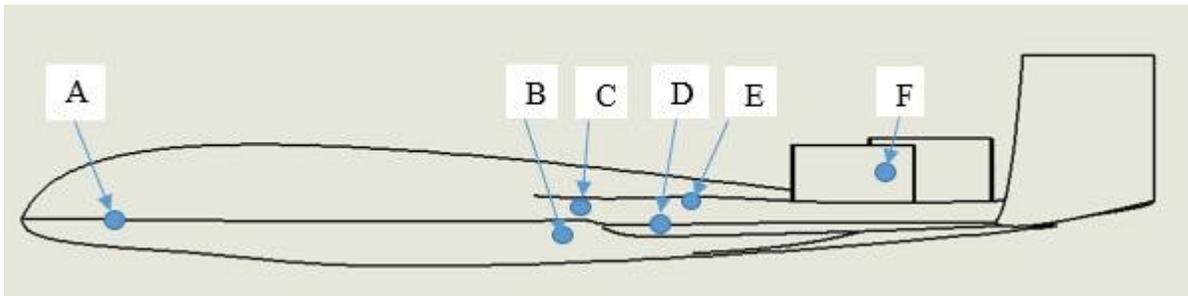
Figure 34: Point masses Locations

Center of gravity calculations:

The center of gravity locations must be calculated for all feasible loading scenarios. The loading scenarios depend to a large extent on the mission of the airplane. Typical loading combinations applicable to mission designed airplane are:

1. Empty Weight

2. Empty Weight + Fuel

3. Empty Weight + Payload

$$\sum_{i=1}^{n} m_i x_i$$

3. Empty Weight + Payload + Fuel (MTOW)

Center of gravity can be calculated using equation: $CG =$

Where $M = \sum_{i=1}^{n} m_i$

For Empty weight, $X_{CG} = 69.714$ ft

For empty weight +Payload, $X_{CG} = 70.745$ ft

For empty Weight + Fuel, $X_{CG} = 71.295$ FT

For MTOW, $X_{CG} = 71.79$ ft

Condition for static stability for BWB:

For Blended Wing Body configuration equation 31 reduces to

$$= (h - h_0) \tag{34}$$

Or

$$= - \tag{35}$$

Where, K_n is called static margin and defined as simply the non-dimensional distance between the aerodynamic center and the CG location.

$$= h - h = \underline{\qquad} \tag{36}$$

K_n is positive if CG is ahead of aerodynamic center. The only way to get < 0, if $K_n > 0$, this

means locating the CG ahead of the aerodynamic center of the wing.

For BWB 601, all values of are known for equation 36.

From error and trail approximation, $X_{NP} = 75$ ft.

From XFLR 5, MAC $= 56.98$ ft.

Using equation 36, CG excursion diagram can be plotted various loading combinations:
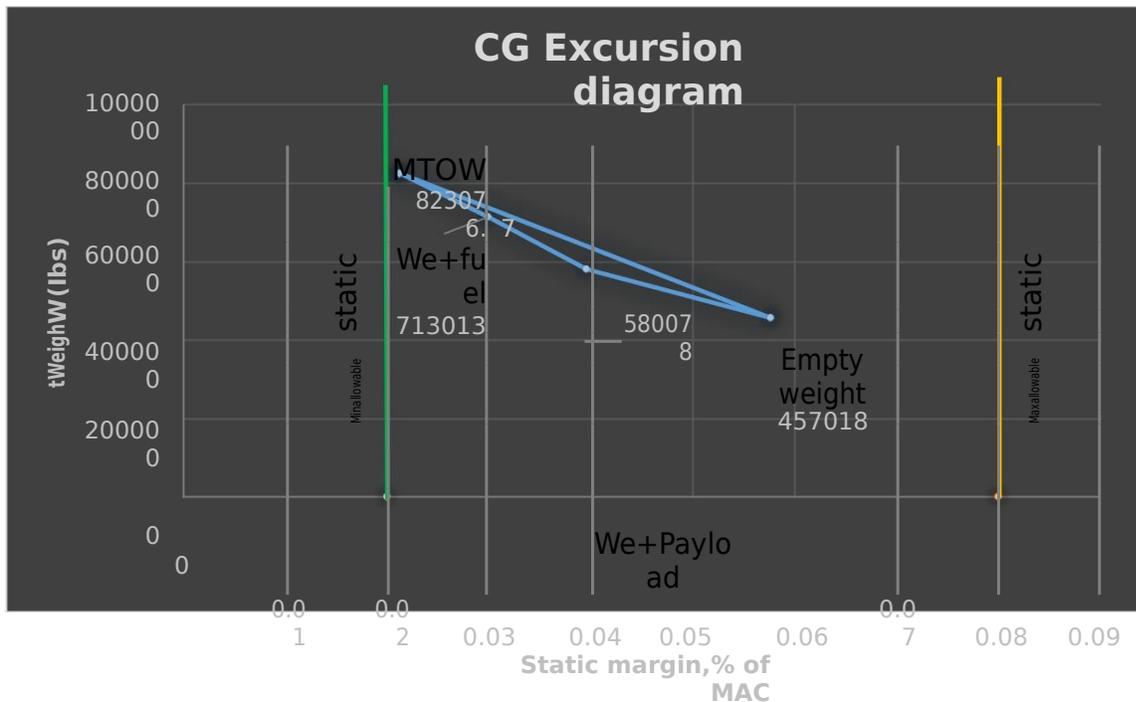
Figure 35: CG excursion diagram

Reference [38] suggests that for tailless aircraft, ultimate static margin is reasonable in range of 0.02 to 0.08. From CG excursion diagram we can see that for various loading combinations, CG lies within this range Thus condition of static stability will be satisfied.

9.0 Dynamic stability and control

9.1 Control surfaces

Control surfaces of tailless aircraft are interesting part of design due to the absence of conventional tail. Tailless aircraft means with or without vertical tail and purely without horizontal tail [35]. The control surfaces for pitch and yaw control for these aircraft are totally different from conventional aircraft. The absence of tail rudder could be substituted by other control surfaces such as split drag flaps, inboard and outboard ailerons, winglets rudders and Thrust Vectoring [35]. The problem of absence of the elevator can solved by substituting it with elevons. The elevons are aircraft control surfaces that serve the functions of both the elevators and the ailerons. They are installed on each side of the aircraft at the trailing edge of the wing. If they elevens on

both side are moved in the same direction they will cause a pitching moment (nose up or down). If moved in opposite direction (one up, one down) they will cause a rolling moment.

For yaw control there are two possible design for BWB aircraft. First one is placing the vertical tail at the tips of wings rather than aft of tail like conventional aircraft. Second one is by using split drag flaps (rudders) as yaw control surfaces.

Split drag flaps consists of upper and lower flaps that will be deflected oppositely. This device works as a drag producer in order to generate yawing moment. Deflection of the flaps on one side of the wing produces asymmetric drag force and, as consequences, yawing moment is produced that rotates the nose of the aircraft toward the deflected flaps. To improve the effectiveness of split flaps they are located near to the wing tips. This provides long moment arm and will give greater yawing moment for the BWB aircraft.

For BWB 601, combination of both wing tip rudder and split drag flaps are proposed considering the reliability and safety issues. Similar configuration was used in Boeing X-48B experimental aircraft and proved to be successful for blended wing body. BWB 601 will have 8 control surfaces, named 1 to 8 as shown in figure 40. For preliminary design, it is assumed that all the flaps or control surfaces have hinge points at x position 80 % chord length and y position 50 % thickness.
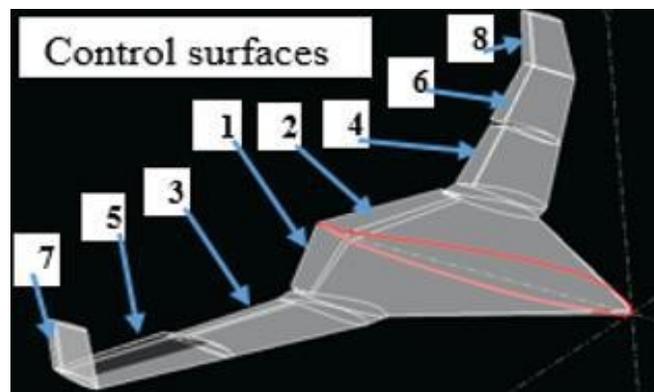
Figure 36: BWB 601 control surfaces

9.2 Longitudinal, lateral and control derivatives

To get stability and control derivatives BWB-601 was model in XFLR5 and simulation was performed as shown in figure 37.

	y (ft)	chord (ft)	offset (ft)	dihedral	twist(°)	foil	X-panels	X-dist	Y-panels	Y-dist
1	0.000	117.000	0.000	0.0	0.00	NACA 23112 with flaps @90% chord	25	Cosine	20	Cosine
2	38.000	36.000	63.000	0.0	0.00	NACA 23112 with flaps @80% chord	13	Cosine	3	Cosine
3	38.000	36.000	63.000	0.0	0.00	NACA 23112	13	Cosine	3	Cosine
4	45.000	34.000	65.000	0.0	0.00	WORTMANN FX 60-126 AIRFOIL	13	Cosine	7	Cosine
5	45.000	34.000	65.000	0.0	0.00	WORTMANN FX 60-126 AIRFOIL with flaps	13	Cosine	6	Cosine
6	82.500	26.000	87.500	0.0	0.00	WORTMANN FX 60-126 AIRFOIL with flaps	13	Cosine	6	Cosine
7	82.500	26.000	87.500	3.0	-4.00	WORTMANN FX 60-126 AIRFOIL with flaps	13	Cosine	6	Cosine
8	120.000	18.000	110.000	0.0	-4.00	WORTMANN FX 60-126 AIRFOIL with flaps	13	Cosine	25	Cosine
9	120.000	18.000	110.000	90.0	-4.00	NACA 0012-34 with flaps	13	Cosine	7	Cosine
10	140.000	15.000	113.000		0.00	NACA 0012-34 with flaps				
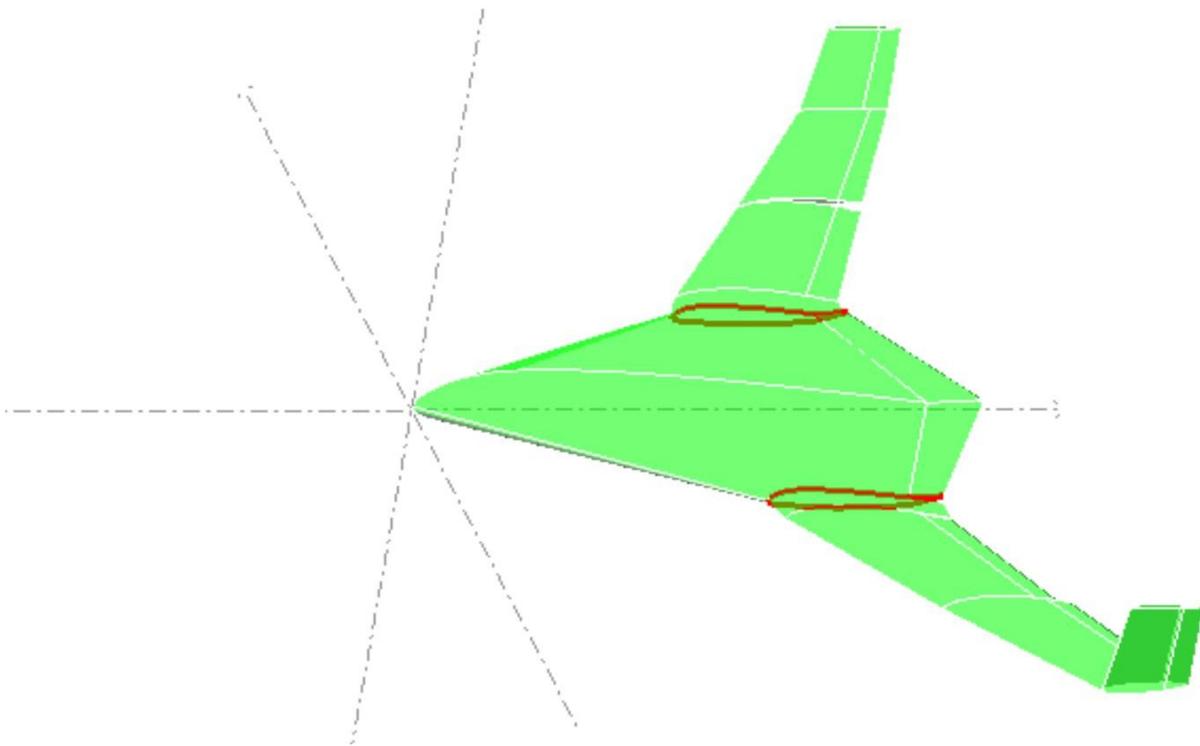
Figure 37: Modelling of BWB601 in XFLR-5

Dimensionless derivatives obtained from XFLR5 simulation are presented in table 22.

Table 22: Dimensionless Aerodynamic stability and control derivatives

Longitudinal Derivatives		Lateral derivatives		Control derivatives	
X_u = -1396		Y_v = -13817		X_{de} = -13622	
X_w = 7398.5		Y_p = -3.0524e+05		Y_{da} = 1.6213e+06	
Z_u = -36600		Y_r = 2.1865e+05		Z_{de} = 3.5829e+06	
Z_w = -3.6782e+05		L_v = -5.5163e+05		L_{da} = 1.0527e+08	
Z_q = -2.9603e+06		L_p = -9.7693e+07		M_{de} = -3.8566e+07	
M_u = -4.6794e-05		L_r = 2.0507e+07		N_{dr} = -2.7629e+07	
M_w = -1.872e+05		N_v = 1.9436e+05			
M_q = -1.7281e+07		N_p = -9.9659e+05			
		N_r = -3.8169e+06			

State matrices and control matrices obtained are as follows:

Longitudinal state matrix

$$
\begin{bmatrix}
-0.0038 & 0.0205 & 0.000 & -9.8100 \\
-0.1016 & -1.0211 & 184.875 & \text{---} \\
0.000 & -0.00111 & -1.0298 & 0.0003 \\
0.000 & 0.000 & 1.000 & 0.000\,0
\end{bmatrix}
\tag{37}
$$

Lateral state matrix

$$
\begin{bmatrix}
-0.0383 & -0.8474 & -192.48 & 9.8100 & 0.0000 \\
-0.0426 & -7.4474 & 1.5762 & 0.0000 & 0.0000 \\
0.0083 & -1.3957 & -1.1953 & 0.0000 & 0.0000 \\
0.000 & 1.0000 & 0.0000 & 0.0000 & 0.0000 \\
0.000 & 0.0000 & 1.0000 & 0.0000 & 0.0000
\end{bmatrix}
\tag{38}
$$

Longitudinal control matrix

$$
\begin{bmatrix}
-0.03781944 \\
-9.967235 \\
-2.298476 \\
0
\end{bmatrix}
\tag{39}
$$

Lateral control matrix for control surfaces 3 and 4

$$
\begin{bmatrix}
11.12483 & 1.018988 \\
&
\end{bmatrix}
\tag{40}
$$

Lateral control matrix for control surfaces 5 and 6

$$-1.019019 \qquad\qquad\qquad (41)$$

$$\left[\begin{matrix}-10.13030\\\vdots\end{matrix}\right]$$

Lateral control matrix for control surfaces 7 and 8

$$-4.501331 \qquad\qquad\qquad (42)$$

$$\left[\begin{matrix}-0.13603\\\vdots\end{matrix}\right]$$

9.3 Dynamic Stability Analysis

The aircraft is said to be dynamically stable if, it eventually returns to equilibrium after being perturbed from initial equilibrium. The difference between Static stability and dynamic stability is that, the static stability deals with the question of how the system will behave in the very short time just after the disturbance, whereas dynamic stability deals with aircraft behavior over long periods of time. In order to conduct dynamic analysis we investigate the motion that occurs after some initial perturbation is applied and from the properties of the motion we can infer or deny stability. It if turns out that the perturbed motion consists of oscillations of increasing amplitude and rapidly increasing departure from the equilibrium state, the aircraft is dynamically unstable; otherwise it is stable. For aircraft dynamic analysis, generally the equations of motion (E.O.M) are developed and then they are solved systematically to observe the time response of various parameters of motion. Space state is one of the convenient ways to describe the EOM and it can be used very effectively in Matlab to observe the time response of aircraft. On the basis of data obtained from XFLR5 both longitudinal and lateral dynamic stability analysis was conducted using Matlab.

9.3.1 Longitudinal Dynamic Stability Analysis

Longitudinal dynamic analysis deals with study of aircraft behavior in longitudinal direction. It includes the parameters: velocity of aircraft along body axis (u), velocity of aircraft

perpendicular to body axis (w), pitch rate (q) and pitch angle (Θ). State space representation of equations of motion of BWB601:

$$
\begin{bmatrix}
-0.0038 & 0.0205 & 0.000 & -9.8100 \\
-0.0156 & -1.0211 & 146.875 & 0.0000 \\
0.000 & -0.00111 & -1.0299 & 0.0000 \\
0.000 & 0.000 & 1.000 & 0.0000
\end{bmatrix}
\begin{bmatrix} \end{bmatrix}
+
\begin{bmatrix}
-0.0378 \\
-0.8471 \\
-0.0866 \\
0
\end{bmatrix}
[\ ]
\tag{43}
$$

Response Transfer functions are obtained by using Matlab and they can be written as:

$$
\frac{(\ )}{(\ )} = \frac{-0.037819\,(s+22.29)\,(s-16.42)\,(s+1.585)}{(s^2 + 0.002212s + 0.003569)\,(s^2 + 2.053s + 3.116)}
\tag{44}
$$

$$
\frac{(\ )}{(\ )} = \frac{-9.9471\,(s+43.75)\,(s^2 + 0.003746s + 0.005265)}{(s^2 + 0.002212s + 0.003569)\,(s^2 + 2.053s + 3.116)}
\tag{45}
$$

$$
\frac{(\ )}{(\ )} = \frac{-2.2985\ (\ +0.9707)\ (\ +0.006054)}{(\ ^2 + 0.002212\ + 0.003569)\,(\ ^2 + 2.053\ + 3.116)}
\tag{46}
$$

$$
\frac{(\ )}{(\ )} = \frac{-2.2985\ (\ +0.9707)(\ +0.006054)}{(\ ^2 + 0.002212\ + 0.003569)\,(\ ^2 + 2.053\ + 3.116)}
\tag{47}
$$

It can be observed from all transfer functions that they have a common denominator and this common denominator represents the characteristic equation when equated to zero. Characteristic equation governs the stability of aircraft and it provides all the important information required for system dynamic stability analysis. Each transfer function has different numerator which governs the magnitude of dynamic stability of each parameter. The characteristics equation for longitudinal dynamics of BWB601 is given by:

$$
\Delta(s) = (\ ^2 + 0.002212\ + 0.003569)\,(\ ^2 + 2.053\ + 3.116) = 0
\tag{48}
$$

First part of characteristic equation gives a pair of complex roots that describes the

phugoid stability mode with following characteristics:

Damping ratio (ζp) = 0.00959

Un-damped natural frequency (ωp) =0.0807 rad/sec

Second part of characteristic equation gives a pair of complex roots that describes the short period stability mode with following characteristics:

Damping ratio (ζs) = 0.579

Un-damped natural frequency (ωs) = 1.313 rad/sec

Both the modes, phugoid and short period mode are aerodynamically stable, however their damping ratios are un-acceptably low. To better under the behavior of aircraft we plotted the time response for transfer functions. For analysis we applied 1° degree elevator input both as a tep and impulse and results are plotted by using Matlab. Fig 1 and 2 shows the time response of aircraft for unit step and unit impulse elevator input respectively. .
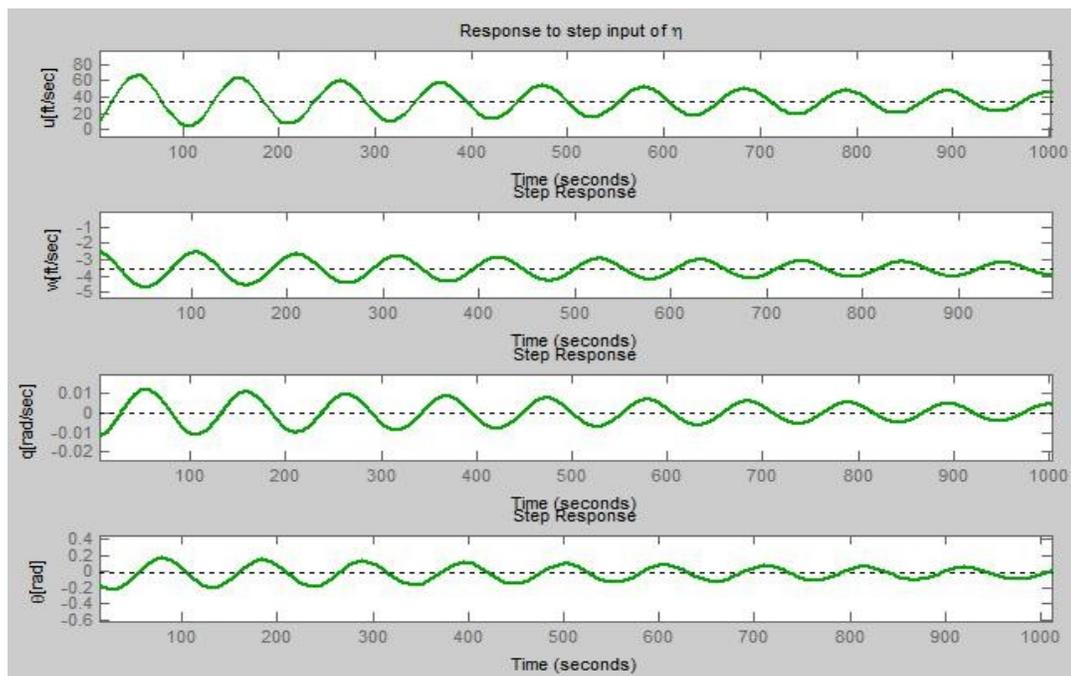
Figure 37: Time response for unit step of elevator
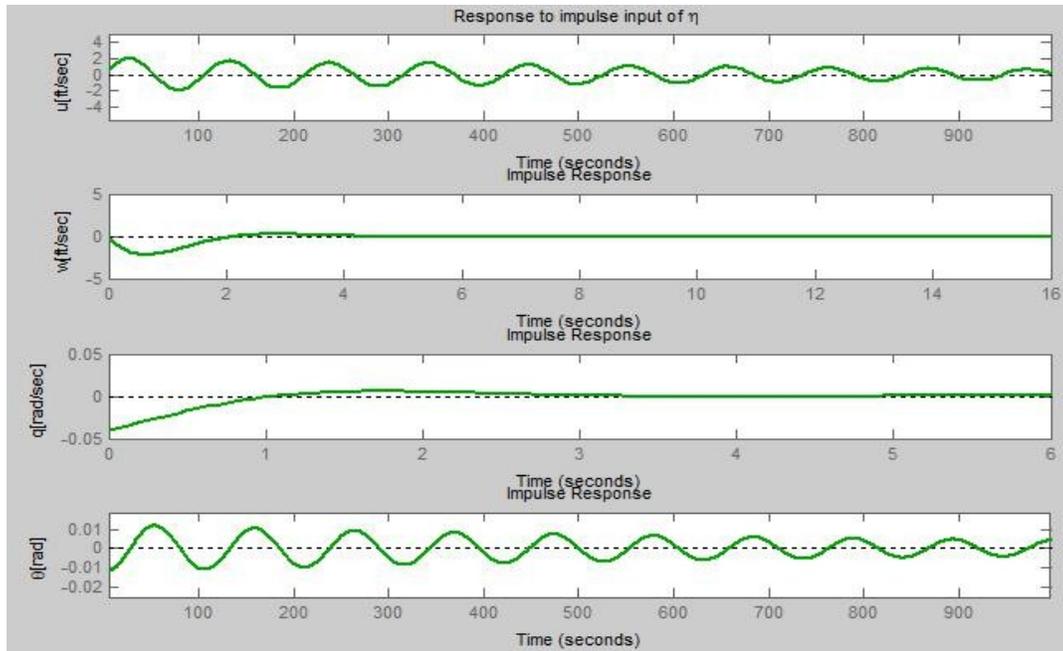
Figure 38: Time response for unit impulse of elevator

From graphs for unit step elevator input: the phugoid oscillations can be observed in all variables, however the magnitude of each stability mode differs in each response variable. Clearly the stability of responses is same as determined by common denominator but magnitude of each response is different which is determined by the unique numerator of the transfer function. For impulse input both phugoid and short period mode can be observed: phugoid mode is visible in u and Θ variables whereas in w and q short period mode is visible. It can be seen that for phugoid mode u and Θ, oscillations takes long time to die out and for short period modes in q and w variable oscillations dies out rather quickly.

9.3.2 Lateral/Directional Static Stability Analysis

Lateral or directional dynamic analysis deals with study of aircraft behavior in lateral direction. It includes the parameters: velocity of aircraft along lateral axis (v), roll rate (p) and yaw rate (r), roll angle (ϕ) and yaw angle (φ). State space matrices of our given lateral system dynamics as

$$\begin{bmatrix} \dot{} \\ \dot{} \\ \dot{} \\ \dot{} \\ \dot{} \end{bmatrix} = \begin{bmatrix} -0.0383 & -0.8474 & -192.48 & 9.81 & 0 \\ -0.0026 & -7.6474 & 1.5742 & 0 & 0 \\ 0.0083 & -0.2807 & -0.1953 & 0 & 0 \\ 0 & 1 & 0 & 0 & 0 \\ 0 & 0 & 1 & 0 & 0 \end{bmatrix} \begin{bmatrix} \\ \\ \\ \\ \end{bmatrix} + \begin{bmatrix} 1.0189 & -1.0190 & -4.5013 \\ 10.1298 & -10.1508 & -0.1266 \\ -0.7350 & 0.7354 & 1.2792 \\ 0 & 0 & 0 \\ 0 & 0 & 0 \end{bmatrix} \begin{bmatrix} \\ \\ \end{bmatrix} \tag{49}$$

Using matlab, transfer functions with respect to control surfaces were obtained to investigate lateral dynamics.

Transfer functions with respect to control surfaces 3 and 4:

$$\frac{(\ )}{(\ )} = \frac{1.019\ (\ +133.6)\ (\ +4.438)\ (\ +0.01333)}{(\ +7.478)\ (\ -0.004675)\ (\ ^2 + 0.2082\ +1.358)} \tag{50}$$

$$\frac{(\ )}{(\ )} = \frac{10.13\ ^2\ (\ ^2 + 0.1151\ +1.017)}{(\ +7.478)\ (\ -0.004675)\ (\ ^2 + 0.2082\ +1.358)} \tag{51}$$

$$\frac{(\ )}{(\ )} = \frac{-0.73501\ (\ +3.511)\ (\ +0.5)\ (\ -0.4055)}{(\ +7.478)\ (\ -0.004675)\ (\ ^2 + 0.2082\ +1.358)} \tag{52}$$

$$\frac{\varnothing(\ )}{(\ )} = \frac{10.13\ (\ ^2 + 0.1151\ +1.017)}{(\ +7.478)\ (\ -0.004675)\ (\ ^2 + 0.2082\ +1.358)} \tag{53}$$

$$\frac{(\ )}{(\ )} = \frac{-0.73501\ (\ +3.511)\ (\ +0.5)\ (\ -0.4055)}{(\ +7.478)\ (\ -0.004675)\ (\ ^2 + 0.2082\ +1.358)} \tag{54}$$

Transfer functions with respect to control surfaces 5 and 6:

$$\frac{(\ )}{(\ )} = \frac{-1.019\ (\ +133.7)\ (\ +4.439)\ (\ +0.01331)}{(\ +7.478)\ (\ -0.004675)\ (\ ^2 + 0.2082\ +1.358)} \tag{55}$$

$$\frac{(\ )}{(\ )} = \frac{-10.131\ ^2\ (\ ^2 + 0.115\ +1.017)}{(\ +7.478)\ (\ -0.004675)\ (\ ^2 + 0.2082\ +1.358)} \tag{56}$$

$$\frac{(\ )}{(\ )} = \frac{0.73541\ (\ +3.513)\ (\ +0.4997)\ (\ -0.4053)}{(\ +7.478)\ (\ -0.004675)\ (\ ^2 + 0.2082\ + 1.358)} \tag{57}$$

$$\frac{\varnothing(\ )}{(\ )} = \frac{-10.131\ (\ ^2 + 0.115\ + 1.017)}{(\ +7.478)\ (\ -0.004675)\ (\ ^2 + 0.2082\ + 1.358)} \tag{58}$$

$$\frac{(\ )}{(\ )} = \frac{0.73541\ (\ +3.513)\ (\ +0.4997)\ (\ -0.4053)}{(\ +7.478)\ (\ -0.004675)\ (\ ^2 + 0.2082\ + 1.358)} \tag{59}$$

Transfer functions with respect to control surfaces 7 and 8:

$$\frac{(\ )}{(\ )} = \frac{-4.5013\ (\ +54.82)\ (\ +5.998)\ (\ -0.002841)}{(\ +7.478)\ (\ -0.004675)\ (\ ^2 + 0.2082\ + 1.358)} \tag{60}$$

$$\frac{(\ )}{(\ )} = \frac{-8.1267\ ^2\ (\ ^2 - 0.03804\ + 0.3168)}{(\ +7.478)\ (\ -0.004675)\ (\ ^2 + 0.2082\ + 1.358)} \tag{61}$$

$$\frac{(\ )}{(\ )} = \frac{1.2793\ (\ +5.661)\ (\ +0.1405)\ (\ -0.1287)}{(\ +7.478)\ (\ -0.004675)\ (\ ^2 + 0.2082\ + 1.358)} \tag{62}$$

$$\frac{\varnothing(\ )}{(\ )} = \frac{-8.1267\ (\ ^2 - 0.03804\ + 0.3168)}{(\ +7.478)\ (\ -0.004675)\ (\ ^2 + 0.2082\ + 1.358)} \tag{63}$$

$$\frac{(\ )}{(\ )} = \frac{1.2793\ (\ +5.661)\ (\ +0.1405)\ (\ -0.1287)}{(\ +7.478)\ (\ -0.004675)\ (\ ^2 + 0.2082\ + 1.358)} \tag{64}$$

Similar to longitudinal dynamics we have a common denominator in all transfer functions, which governs the lateral dynamics stability of the A/C, while the numerators are different for each transfer function and they govern the magnitude of each stability response.

Using matlab the time response for impulse input are plotted for all transfer functions as shown in fig 39, 40 and 50.
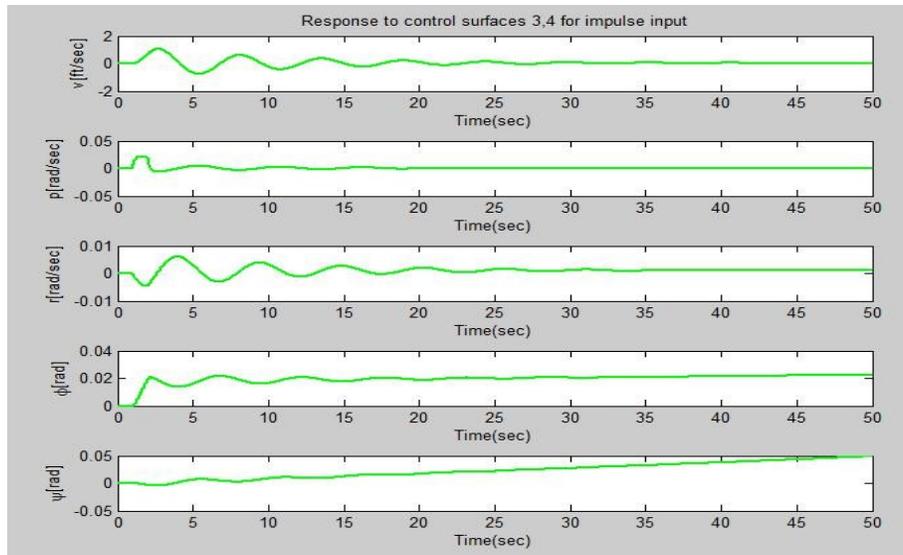
Figure 39: Time response for impulse input of 3 and 4 surfaces
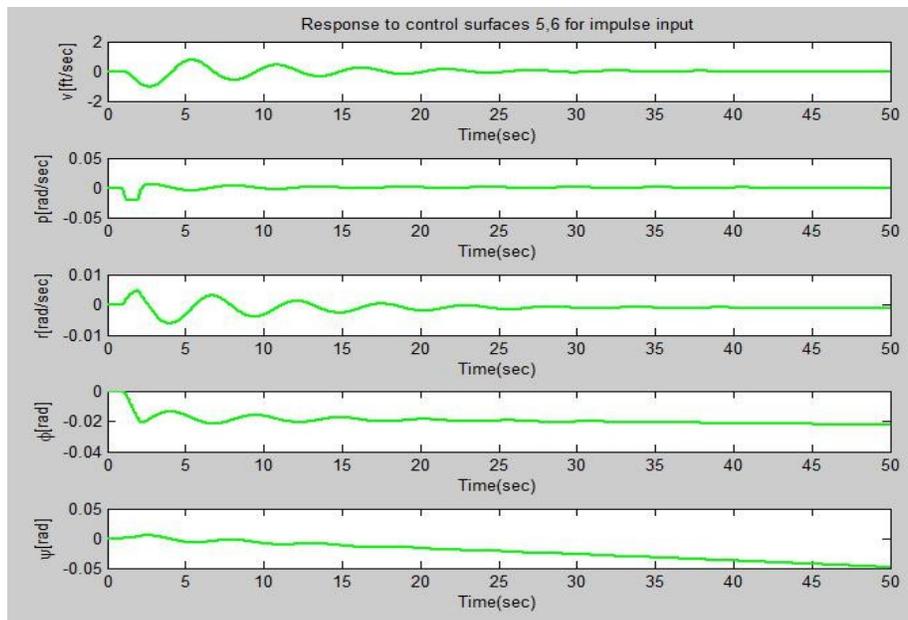
Figure 40: Time response for impulse input of 5 and 6 surfaces

Figure 41: Time response for impulse input of 7 and 8 surfaces

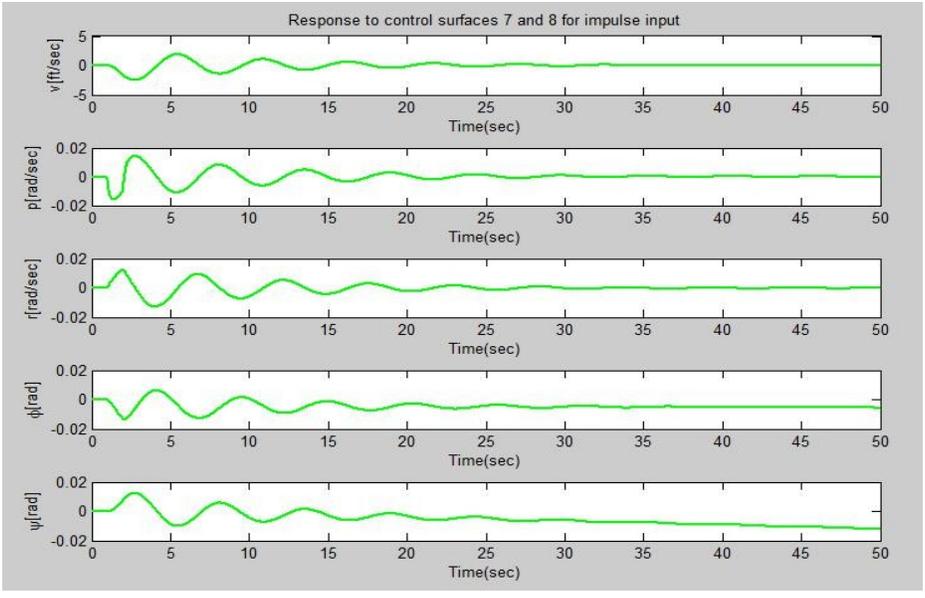It can be seen clearly from above graphs, that after initial disturbance in v, p r, ф oscillations eventually will converge and settle down around an equilibrium point. In other words system dynamics are stable in there variables. However for yaw angle (φ) graphs indicates that the system dynamics are marginally stable or neutrally stable.

10.0 BWB 601 Drag estimation.

Drag force is combination of all forces that resist against aircraft motion and is given by following equation.

$$= \quad \frac{1}{2}^{2} \tag{65}$$

Where C_D is drag coefficient. It is a non-dimensional parameter that takes into account every aerodynamic configuration aspect of the aircraft including wing, tail, fuselage engine, control surfaces, landing gear, rivets and antenna etc.

Total drag is the sum of induced drag (D_i) and zero lift drag (D_o)

$$= \quad + \tag{66}$$

Induced drag is the drag directly related to production of lift. In other words it depends upon angle of attack of the aircraft (i.e. lift coefficient). As the angle of attack of the aircraft varies, this type of drag is changed. The induced drag in itself include drag due to vortices and air compressibility. In low subsonic flight, compressibility drag is negligible, but is high subsonic and transonic flight, must be taken into account. In supersonic flight, wave drag is added to the induced drag. The reason is to account for the contribution of shock wave. The induced drag is a function of airspeed, air density, reference area, and the lift coefficient:

$$= \frac{1}{2} \qquad\qquad (67)$$

Zero lift drag doesn't have any influence from lift. The zero-lift drag includes all types of drags that do not depend on production of the lift. Every aerodynamic component of aircraft generates zero-lift drag. Typical components are fuselage, wing, tail, landing gear, engine nacelle, strut and antenna. The zero-lift drag is a given by:

$$= \frac{1}{2} \qquad\qquad (68)$$

In this equation, the coefficient $_0$ is called zero-lift drag coefficient.

From the equations; one can conclude that drag coefficient has two components:

$$= _0 + \qquad\qquad (69)$$

Above equation can be written as (drag polar equation)

$$= _0 + ^2 \qquad\qquad (70)$$

Where k is the induced drag correction factor and it is inversely proportional to the wing aspect ratio and wing Oswald efficiency factor (e).

$$= \frac{1}{\pi} = 0.051366345 \qquad\qquad (71)$$

$$= _0 + 0.0513 \, ^2 \qquad\qquad (72)$$

Procedure for estimation of zero lift drag coefficient

The component built up method was used to estimate zero lift drag coefficient []. According to this technique, drag coefficients of all individual components are added to get total drag coefficient. It takes account of skin friction drag, pressure drag due to viscous separation and interference effects of every component. Miscellaneous drags due to aircraft special features are added to total along with total contribution from leakage and protuberances.

Subsonic zero lift drag according to build up method is given by below equation:

$$= \frac{\Sigma(\ )}{} + \quad + \tag{73}$$

Where "c" subscript indicates that those values are different for each component. is the flat plate skin friction coefficient, and is a non-dimensional number. For turbulent flow it depends upon Reynolds number as follow:

$$= \frac{0.455}{[\ (\ )]^{2.58} (1+0.144\quad)^{2.65}} \tag{74}$$

Where Re is the Reynolds number.

is the component form factor that estimates pressure drag due to viscous drag separation. Form factor for subsonic speed is given by:

For wing, tail, strut and pylon:
$$= [1 + \frac{0.\ 6}{\ }\ (\_\ ) + (\_\ )^4][1.34^{0.18}(\ )^{0.28}] \tag{75}$$

For fuselage and smooth canopy:
$$= 1 + \frac{60}{} + \frac{}{400} \tag{76}$$

For Nacelle and smooth external surface:
$$= 1 + \frac{0.35}{} \tag{77}$$

Where (_) is the chord wise location of airfoil maximum thickness point and = _

$$= 1 + 2.7 \quad \_ + 100 \quad \_^4 \tag{78}$$

is the maximum thickness to chord ratio of the lifting surface.

Q_C in equation is interference factor. It depends upon mutual interference of components.

10.1 Calculations of zero drag coefficient for center body (Inner wing)

For cruise conditions (Altitude=45000 ft)

Density of air (ρ) = 4.62×10^{-4} slug/ft^3

Dynamic viscosity (μ) = 2.969×10^{-7} lbs. /ft^2

Speed of sound (a) =967.5 ft/s

Cruise speed (V=Ma) = 822.4 ft/s

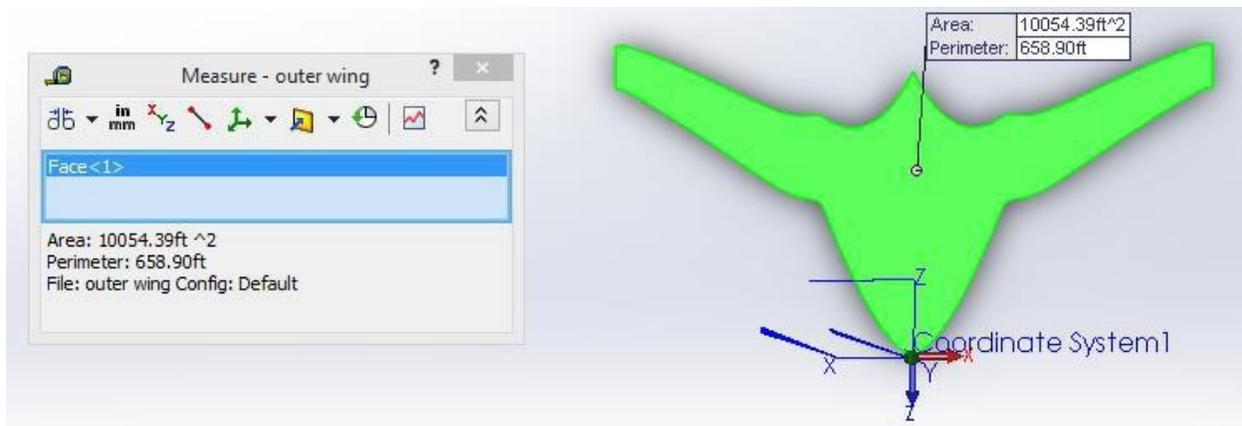Max thickness to chord ratio (t/c) = 0.12

Reference area is taken as projected area of center body + projected area of outer wing)

Reference area and S_{wet} for center body is evaluated from solid work model (Fig & fig).

Reference area= 10054.39 ft^2.

S_{wet} for center body= 2x5626.87 = 13053.74 ft^2.

Figure 42: Measurement of projected area of center body and outer wing from solid work model

Figure 43: Measurement of wet area of Center body from solid work model

Mean aerodynamic chord for center body is calculated by equation:

$$\bar{c} = \frac{2}{3} [1 + \ldots - \ldots] = 85.53 \tag{79}$$

$$\ldots = 1.09E+08 \tag{80}$$

From equation () $= \dfrac{0.455}{\ldots} = 1.93E-03$ (81)

From equation () $= [1 + \dfrac{0.6}{\ldots} (\_) + (\_)^4][1.34^{0.18}(\ldots)^{0.28}] = 1.51E+00$ (82)

Also $Q_{cb}=1$ (lifting body)

Zero drag coefficient for center body $= \underline{\qquad\qquad} = 0.0038$ (83)

10.2 Calculations of zero drag coefficient for outer wing

S_{wet} for outer wing = Total wet area of wing and center body– Wet area of center body

= 2x10470 -13053.74 = 7887 ft^2

Figure 44: Measurement of wet area of wing + center body from solid work model

Mean aerodynamic chord for outer wing is calculated by equation:

$$\bar{c} = \frac{2}{3}[1 + - \quad \underline{\quad\quad}] = 28 \tag{84}$$

$$\underline{\quad\quad} = 3.57E+07 \tag{85}$$

From equation () $= \dfrac{0.455}{\quad\quad\quad\quad\quad} = 2.26E\text{-}03$ (86)

From equation () $= [1 + \dfrac{0.6}{\quad} (\bar{\quad}) + (\bar{\quad})^4][1.34^{0.18}(\quad)^{0.28}] = 1.62E+00$ (87)

Also Q_ow=1 (lifting body)

Zero drag coefficient for outer wing, $\underline{\quad\quad\quad\quad\quad} = \quad = 0.0029$ (88)

10.3 Calculations of zero drag coefficient for Winglets

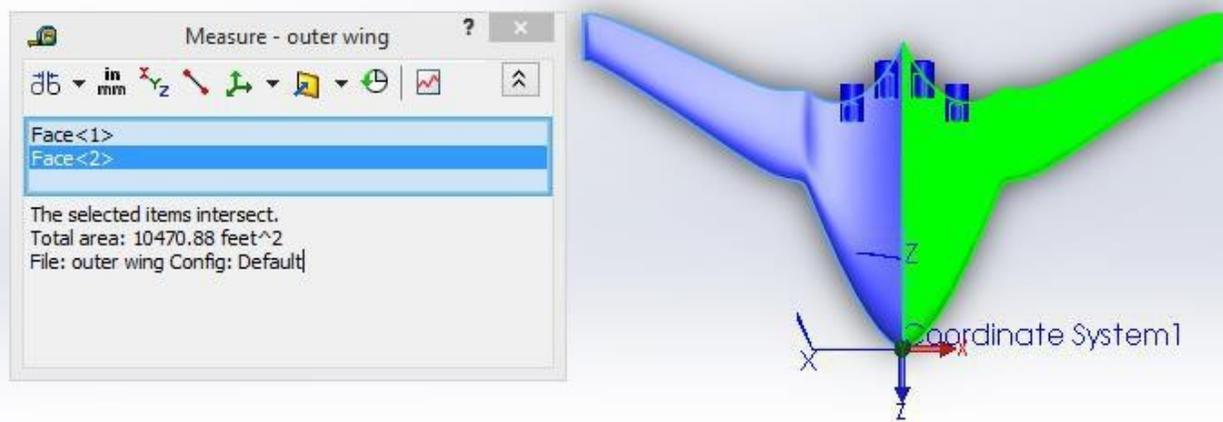S_{wet} for winglet = 1211.32 ft^2 (from solid work model)
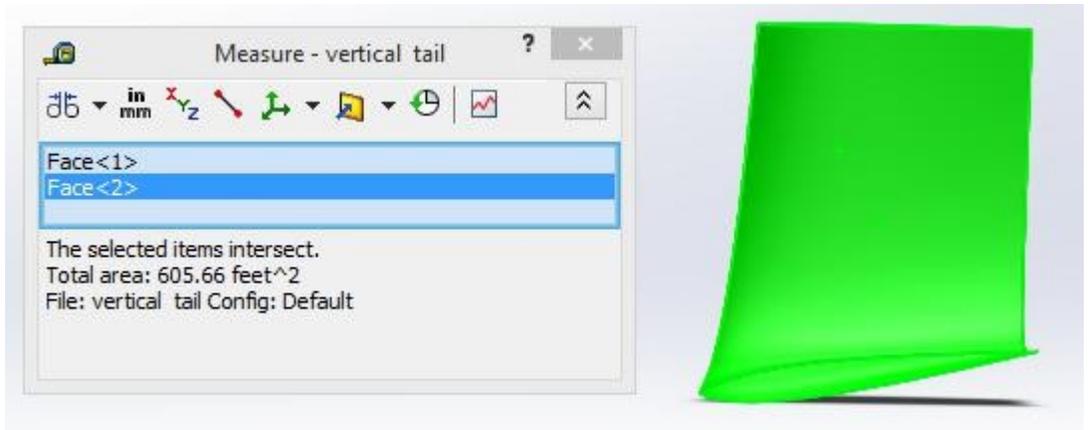
Figure 45: Measurement of Wet area of a winglet from solid work model

Mean aerodynamic chord for outer wing is calculated by equation:

$$\frac{2}{}[1 + - \underline{\quad\quad}] = 16.54 \tag{89}$$

$$\underline{\quad\quad} = 2.11\text{E}{+}07 \tag{90}$$

From equation ( ) $\quad = \dfrac{0.455}{\underline{\hspace{3cm}}} = 2.45\text{E}{-}03$ $\tag{91}$

From equation ( ) $\quad = [1 + \dfrac{0.6}{-}(\bar{\ }) + (\bar{\ })^4 \ ][1.34^{0.18}(\quad)^{0.28}\ ]$ $= 1.66\text{E}{+}0\,0$ $\tag{92}$

Also Q_w=1 (lifting body)

Zero drag coefficient for winglet, $\quad = \underline{\hspace{2.5cm}} = 0.0005$ $\tag{93}$

10.4 Calculations of zero drag coefficient for Nacelle

S_{wet} for Nacelle = 4x347.64**1390.56** ft^2 (from solid work model)
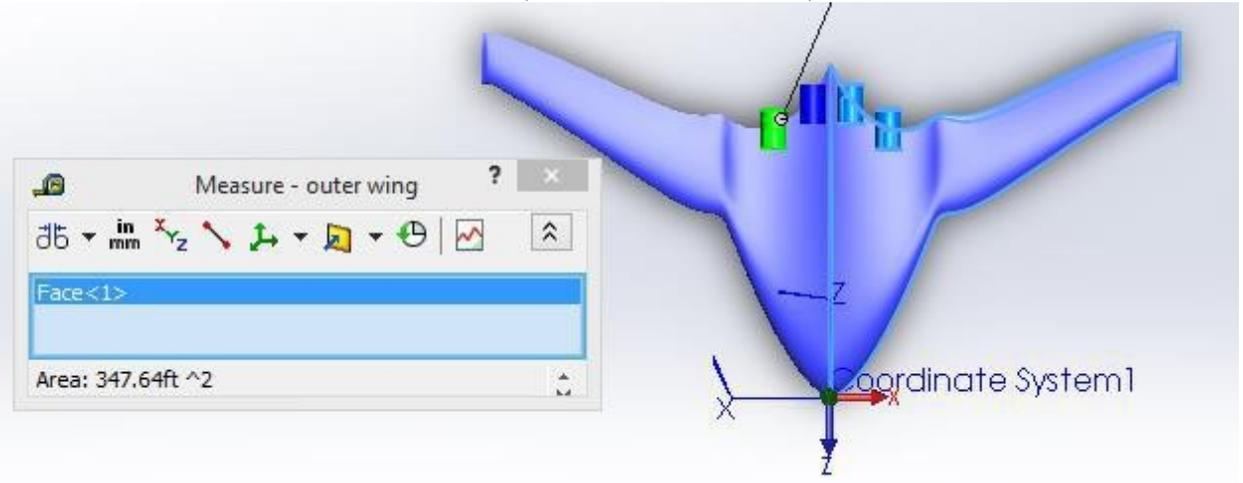
Figure 46: Measurement of Wet area of a winglet from solid work model

Length of Nacelle (L_n) = 15ft

$$= \underline{\quad\quad} = 1.91E+07$$

From equation () $- \;= \dfrac{0.455}{\underline{\qquad\qquad}} \begin{array}{l}= 2.49E\text{-}\\03\end{array}$

(94)

From equation () $= 1 + \dfrac{0.35}{\underline{\quad}}\, 1.18E+00$

(95)

From reference interference factor between nacelle and center body, $Q_w=1.3$

Zero drag coefficient for Nacelle, $\underline{\qquad\qquad} = \quad - \quad = 0.0005$

(96)

10.5 Total zero lift coefficient

Total drag coefficient was obtained from summation of drag coefficients of all components and adding miscellaneous and leakage & protuberance drag. Assuming, $\_$ = 10% of $_0$

$_{\&} \; _{= 4\% \, of} \quad _0$

$$= \frac{\Sigma(\ )}{} + \quad + \tag{97}$$

$$_0 = 0.0077 + 0.10 + 0.04 \tag{98}$$

$$_0 = 0.009$$

10.6 Drag polar

From equation 1 and 2 we get

$$= 0.009 + 0.0513 \; ^2 \tag{99}$$

Drag polar for BWB-601 is presented in figure
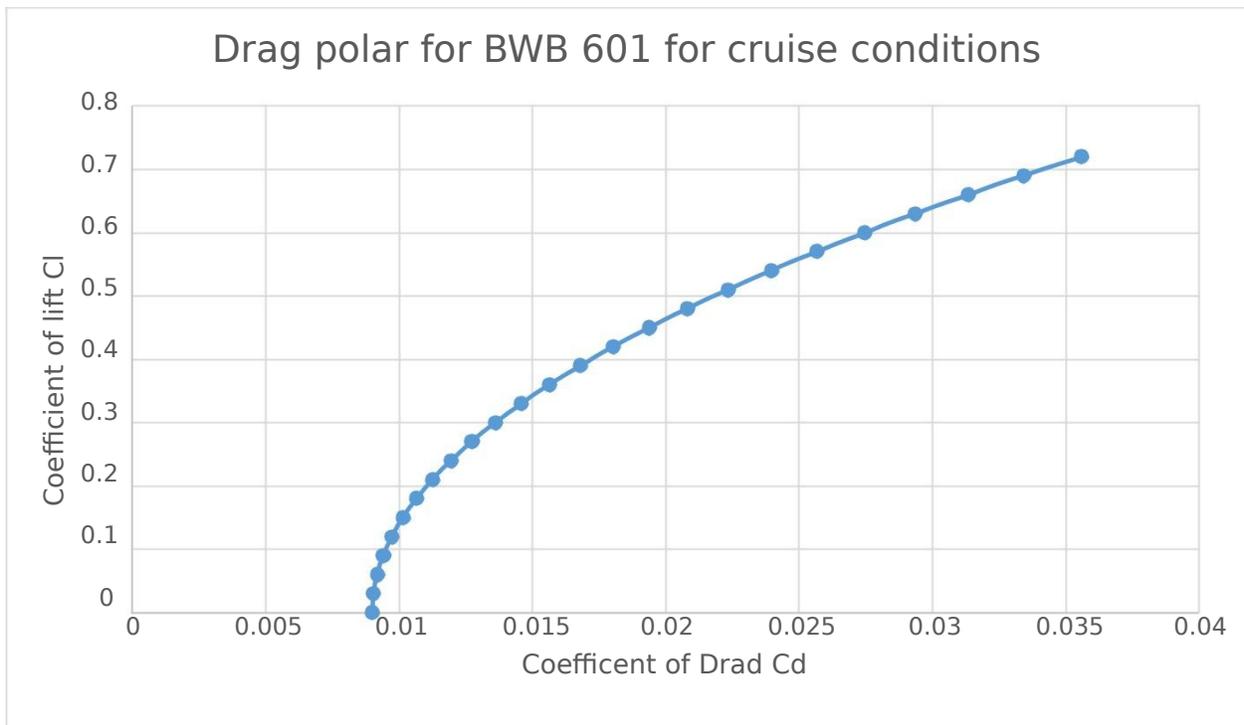
Figure : Drag polar for BWB 601

10.0 Conclusions or Discussions

To meet the goals of green aviation: fuel efficiency, emissions and noise, there is a definite need of new solutions. Although, there are number of alternatives including engine modifications, alternative fuels, and changing accent & decent approach but nothing seems as promising as BWB aircraft. Preliminary sizing of BWB 601 shows the weight saving of 19.8 percent in comparison to Boeing 747-8I for almost same payload. Placing of engine over the center body offered the noise shielding from ground. The advances in flight and control technology have made it possible to fly BWB as safer as like that of conventional configuration. Dynamic stability and control analysis has proven that BWB601 is controllable and safe to fly.

In future work, CFD analysis can be done using real CFD software's like Ansys Fluent to predict the aerodynamic gains of BWW601 configuration.

References

1. AID Airfoil Investigation Database. (n.d.). Retrieved from *http://www.airfoildb.com/foils/401*

2. Bowlers, A. (2000, 09). Blended wing body design challenges of 21 century. The wing is the thing meeting. Retrieved from *http://www.twitt.org/BWBBowers.html6.*

3. Basic design of flying wing models. (n.d.). Retrieved from

http://www.aerodesign.ufsc.br/ipa/03_design/basic_design_of_flying_wing models.doc

4. Bradley, K. B. NASA, (2004). A sizing methodology for the conceptual design of blended-wing-body transports. Retrieved from

http://ntrs.nasa.gov/archive/nasa/casi.ntrs.nasa.gov/20040110949.pdf 5.

"Burnelli." *Burnelli*. Aerofiles, 10 Oct. 2008. Web. 4 Feb. 2014.

<http://www.aerofiles.com/_burnelli.html>.

6. *Burnelli rb-1*. (n.d.). Retrieved from http://en.wikipedia.org/wiki/Burnelli_RB-110.

7. Chambers, J. NASA, (n.d.). Innovation in flight: Research of the NASA Langley research center on revolutionary advanced concepts for aeronautics. Retrieved from website:

8. European Aviation Safety Agency, (2013). *EASA type-certificate data sheet* (E.012). Retrieved from website*: http://www.easa.europa.eu/system/files/dfu/EASA-TCDS-E.012_Rolls-- Royce_plc._RB211_Trent_900_series_engines-06-11122013.pdf*

9. Frischling, S. Flying with fish the blog for those who fly & those who want to fly smarter [Web log message]. Retrieved from *http://boardingarea.com/flyingwithfish/2010/04/03/reader-mail-whats-bigger-the-new-747-8-or-the-a380/*

10. GEnx turbofan engine "The next generation of engine. (n.d.). Retrieved from

http://www.mtu.de/de/products_services/new_business_commercial/programs/genx/GEnx.pdf

11. GENX Aircraft Engine. (n.d.). Retrieved from

http://www.ecomagination.com/portfolio/genx-aircraft-engine

12 Hepperle, M. (n.d.). Flying wings. Retrieved from *http://www.mh-aerotools.de/airfoils/*

13 Hamburg, W. & Angewandte, H, (2007). A student project of blended wing body aircraft

from conceptual design to testing. (Master's thesis)Retrieved from http://www.mp.haw-

hamburg.de/pers/Scholz/ewade/2007/EWADE2007_Scholz.pdf8.

14 Journal of Aircraft vol.41, No 1, January–February2004 Design of the Blended Wing Body

Subsonic Transport R. H. Liebeck, the Boeing Company, Huntington Beach, California 92647

15 Kisska, M., & Princen, N. (n.d.). X-48B Flight Research – Test Progress and Instrumentation

Needs for the Future. . Retrieved April 13, 2014, from

16. Koehler, T. (n.d.). Boeing X-48C blended wing body research aircraft completes flight

testing. Retrieved from *http://boeing.mediaroom.com/index.php?s=20295&item=128631*

17. List of airliners by maximum takeoff weight33. (n.d.). . Retrieved March 8, 2014, from

http://en.wikipedia.org/wiki/List_of_airliners_by_maximum_takeoff_weight33.

18. NASA Armstrong fact sheet (2014). : X-48 hybrid / blended wing body. Retrieved from

website: *http://www.nasa.gov/centers/dryden/news/FactSheets/FS-090-DFRC.html*

19. "NORTHROP YB-49". National Museum of US Air force, 17 July 2013. Web. 4 May 2014.

<http://www.nationalmuseum.af.mil/factsheets/factsheet.asp?id=2670>.

20. National Aeronautics and space administration, (n.d.). *Wing design*. Retrieved from website:

http://www.aeronautics.nasa.gov/pdf/wing_design_k-12.pdf

21. NASA - Online Center of Gravity Calculator. (n.d.). NASA - Online Center of Gravity Calculator. Retrieved May 1, 2014, from *http://www.nasascale.org/howtos/cg-calculator.htm*

22. Over 29,000 new aircraft required in the next 20 years. (n.d.). Retrieved from *http://www.airbus.com/presscentre/pressreleases/press-release-detail/detail/over-29000-new-aircraft-required-in-the-next-20-years/*

23. Parch, A. (n.d.). Directory of US military rockets and missiles appendix 4: Undesignated vehicles X-48. Retrieved from *http://www.designation-systems.net/dusrm/app4/x-48.html4*

24. Roskam, J. (1985). *Airplane design*. Ottawa, Kan.: Roskam Aviation and Engineering Corporation.

25. Rahman, N. (n.d.). Propulsion and flight controls integration for the blended wing body aircraft. (Unpublished doctoral dissertation, Cranfield University). Retrieved from *https://dspace.lib.cranfield.ac.uk/bitstream/1826/4095/1/Ur_Rahman_Thesis_2009.pdf* 26. "Special Report Commercial engines 2012." . N.p., n.d. Web. 4 May 2014. *<http://www.flightglobal.com/.../commercial-engines-2012.pdf>*.

27. Stanford University. Wing lift distribution. (n.d.). Retrieved from *http://adg.stanford.edu/aa241/wingdesign/winglift.html*

28. Simpson, L. (2004, 05 17). Aviation archive: Aviation heritage. Retrieved from *http://www.aviationarchive.org.uk/Gpages/html/G3806.html*

29. Singh, A. (n.d.). Seminar report on blended wing body by akfunworld. Retrieved from *http://www.scribd.com/doc/92463570/Seminar-report-on-Blended-Wing-Body-by-akfunworld*

30. *The GENX family engine*. (n.d.). Retrieved from *http://www.geaviation.com/engines/commercial/genx/*

31. Telusers, E. (n.d.). Boeing 747 8 international 3077 hd wallpapers. Retrieved from

http://telusers.com/boeing-747-8-intercontinental-3077-hd-wallpapers.html

32. Westland dreadnought 1923. (n.d.). Retrieved from

http://www.aviastar.org/air/england/west_dreadnought.php13.

33. Worldwide military. (n.d.). Retrieved from *http://www.worldwide-military.com/Military*

Aircraft/US Bombers/B-2 Spirit_general_EN.htm

34. *Wing design*. (n.d.). Retrieved from *http://mail.tku.edu.tw/095980/6_Wing Design.pdf*

35. Wisnoe, w, & Kuntjoro, w. (2012, June 1). Aerodynamic design and analysis of yaw control

surfaces for uitm BWB baseline-ii UAV. Retrieved April 4, 2014, from

http://eprints.uitm.edu.my/7908/1/LP_PROF%20DR%20WIRACHMAN%20WISNOE%2012_24. pdf

36. Hunter, J. (2014). Aircraft Static stability. *Flight Mechanics* (). San Jose State.

37. Tulapurkara, E. (n.d.). Flight dynamics-I "Performance analysis II – Steady climb, descent and

glide ". Retrieved May 2, 2014, from http://nptel.ac.in/courses/101106041/Chapter%206%20-

%20Lecture%2021%2021-12-2011.pdf

38. Charles, J. (1994, August 19). An interim report on the stability and control of tailless airplanes.

Retrieved October 28, 2014, from http://ntrs.nasa.gov/archive/nasa/casi.ntrs.nasa.gov/200502417

39.pdf

Appendices

Appendix A: Matlab code for longitudinal dynamics

```matlab
% Matlab code for longitudinal dynmics stability of BWB601
clc;
% Defining State Matrix
 A =[-0.00387572    0.0205402      0                -9.81
     -0.101611     -1.02117       184.876            0
      0            -0.0111568     -1.02993            0
      0             0              1                  0    ]
% Defing input matrix
B =[-0.03781944
    -9.947125
    -2.298476
      0            ]
C = eye(4); % C matrix is identity matrix 4x4
D = zeros(length(C),1); % D Matrix is zero matrix 4x1
sys = ss(A,B,C,D);
TF = tf(sys); % This will gives us 4 transfer functions
%  Obtaining tranfer functions and defining each
% tranfer function with clear name and label setting
[num,den]=ss2tf(A,B,C,D);
disp('TF from n --> u')
disp('------------------')
TF_n2u = zpk(tf(num(1,:),den))

disp('TF from n --> w')
disp('------------------')
TF_n2w = zpk(tf(num(2,:),den))

disp('TF from n --> q')
disp('------------------')
TF_n2q = zpk(tf(num(3,:),den))

disp('TF from n --> theta')
disp('------------------')
TF_n2th = zpk(tf(num(4,:),den))

% Plots for step input
figure,
subplot(4,1,1),step(TF_n2u*pi/180,'-g'),ylabel('u[ft/sec]')
title('Response to step input of \eta ')
subplot(4,1,2),step(TF_n2w*pi/180,'-g'),ylabel('w[ft/sec]')
title('Response to step input of \eta ')
subplot(4,1,3),step(TF_n2q*pi/180,'-g'),ylabel('q[rad/sec]')
title('Response to step input of \eta ')
subplot(4,1,4),step(TF_n2th*pi/180,'-g'),ylabel('\theta[rad]')

title('Response to step input of \eta ')
% Plots for impulse input
figure,
```

```matlab
subplot(4,1,1),impulse(TF_n2u*pi/180,'-g'),ylabel('u[ft/sec]')
title('Response to impulse input of \eta ')
subplot(4,1,2),impulse(TF_n2w*pi/180,'-g'),ylabel('w[ft/sec]')
title('Response to impulse input of \eta ')
subplot(4,1,3),impulse(TF_n2q*pi/180,'-g'),ylabel('q[rad/sec]')
title('Response to impulse input of \eta ')
subplot(4,1,4),impulse(TF_n2th*pi/180,'-g'),ylabel('\theta[rad]')
title('Response to impulse input of \eta ')

% Eigenvalues of Long. system dynamics
eig(A)
% Eigenvalues and Eigenvector analysis
[EigVec,EigVal] = eig(A);

for ii = 1:length(A)
    disp(['Eigenvector associated with the ',num2str(ii),' eigenvalue'])
    disp('------------------------------------------')
    EigVal(ii,ii),EigVec(:,ii),
end

%%
% Another important analysis could be conducted by investigating the
% eigenvectors and their amplitude to see the individual effect of each
% mode on state dynamics.
Mag_of_EigVec = [abs(EigVec(:,1))  abs(EigVec(:,2)) ...
                 abs(EigVec(:,3))  abs(EigVec(:,4))];

damp(A)

disp('                    Short Period Mode    |  Phugoid Mode')
disp('             ----------------------------------------------          ')
disp(['u        |          ',num2str(Mag_of_EigVec(1,1:2)),' |
',num2str(Mag_of_EigVec(1,3:4))])
disp(['w        |          ',num2str(Mag_of_EigVec(2,1:2)),'    |
',num2str(Mag_of_EigVec(2,3:4))])
disp(['q        |          ',num2str(Mag_of_EigVec(3,1:2)),' |
',num2str(Mag_of_EigVec(3,3:4))])
disp(['theta    |          ',num2str(Mag_of_EigVec(4,1:2)),' |
',num2str(Mag_of_EigVec(4,3:4))])

% Damping ratio:
damp(A)
```

Appendix B: Matlab code for Lateral dynamics

```matlab
% Matlab code for lateral or directional dynamics anlysis
% First, we will construct the state space matrices of our given lateral
% system dynamics as
clc
clear all
A=[  -0.0383595     -0.847425           -192.488      9.81    0
     -0.0426963      -7.44743             1.57629      0       0
      0.0083637       0.280703           -0.195392     0       0
      0               1                   0            0       0
      0               0                   1            0       0]

B= [ 1.018988       -1.019019        -4.501331
     10.12985        -10.13085        -8.126692
     -0.7350099       0.7354143        1. 279297
      0               0                0
      0               0                0            ];


C = eye(length(A));

D = [ 0 0 0; 0 0 0 ; 0 0 0; 0 0 0; 0 0 0];

% Transfer Functions for ailrons or flaps 3 amd 4:

[num1,den1] = ss2tf(A,B,C,D,1);

disp('TF from ksi(ail) --> v')
disp('------------------ ')
TF_ksi2v = zpk(tf(num1(1,:),den1))

disp('TF from ksi(ail) --> p')
disp('------------------ ')
TF_ksi2p = zpk(tf(num1(2,:),den1))

disp('TF from ksi(ail) --> r')
disp('------------------ ')
TF_ksi2r = zpk(tf(num1(3,:),den1))

disp('TF from ksi(ail) --> phi')
disp('------------------ ')
TF_ksi2phi = zpk(tf(num1(4,:),den1))

disp('TF from ksi(ail) --> psi')
disp('------------------')
TF_ksi2psi = zpk(tf(num1(5,:),den1))

% Transfer Functions for flaps 5 amd 6:

[num2,den2] = ss2tf(A,B,C,D,2);
```

```matlab
disp('TF from zeta(rudder_flap) --> v')
disp('-----------------             ')
TF_zeta2v = zpk(tf(num2(1,:),den2))


disp('TF from zeta(rudder_flap) --> p')
disp('-----------------             ')
TF_zeta2p = zpk(tf(num2(2,:),den2))


disp('TF from zeta(rudder_flap) --> r')
disp('-----------------             ')
TF_zeta2r = zpk(tf(num2(3,:),den2))


disp('TF from zeta(rudder_flap) --> phi')
disp('-----------------             ')
TF_zeta2phi = zpk(tf(num2(4,:),den2))


disp('TF from zeta(rudder_flap) --> psi')
disp('-----------------             ')
TF_zeta2psi = zpk(tf(num2(5,:),den2))
% Transfer Functions for rudder flaps 7 amd 8:
[num3,den3] = ss2tf(A,B,C,D,3);
disp('TF from zeta(rud) --> v')
disp('------------------') TF_zeta2v
= zpk(tf(num3(1,:),den3))


disp('TF from zeta(rud) --> p')
disp('------------------')
TF_zeta2p = zpk(tf(num3(2,:),den3))


disp('TF from zeta(rud) --> r')
disp('------------------')
TF_zeta2r = zpk(tf(num3(3,:),den3))


disp('TF from zeta(rud) --> phi')
disp('------------------')
TF_zeta2phi = zpk(tf(num3(4,:),den3))


disp('TF from zeta(rud) --> psi')
disp('------------------')
TF_zeta2psi = zpk(tf(num3(5,:),den3))


%%
m=eig(A);

% Eigenvalues and Eigenvector analysis
[EigVec,EigVal] = eig(A);

for ii = 1:length(A)
    disp(['Eigenvector associated with the ',num2str(ii),' eigenvalue'])
    disp('----------------------------------------------')
    EigVal(ii,ii),EigVec(:,ii),
end
```

```matlab
% Damping ratio, natural frequency of modes
damp(A)

% Solutions of given Lat. EoMs

t = [0:1e-2:SimTime]; % simulation time vector
u = zeros(length(t),1); % input vector

% Create the step input in matlab
indx_t_1 = find(t == 1); % we need to specifiy when the step input will ramp
up
indx_ t_2 = find(t == 2); % we need to specify when the step input will die
down
%indx_t_ 3 = find(t == 50); % we need to specifiy when the step input will
ramp up
%indx _t_4 = find(t == 51); % we need to specify when the step input will die
down
%indx_t_ 5 = find(t == 75); % we need to specifiy when the step input will
ramp up
%indx_t_6 = find(t == 76);
u_imp_ail = u; % create impulse input for only aileron active
u_imp_rud = u; % create impulse input for only rudder active
u_imp_flap =u;

% Plotting response for control surfaces 3 and 4 for unit impulse input %
And then the next thing is to simulate the results as the following:
u_imp_ail(indx_t_1:indx_t_2,1) = 1*pi/180; % construct impulse input in [RAD]
u_imp_rud(indx_t_1:indx_t_2,1) = 0*pi/180; % construct impulse input in [RAD]
u_imp_flap(indx_t_1:indx_t_2,1) = 0*pi/180;
lat_sys = ss(A,B,C,D);
[y_lsim, t_lsim] = lsim(lat_sys,[u_imp _ail u_imp_rud u_imp_flap],t); %
store all outputs for further investigation

figure,
subplot(5,1,1)
plot(t_lsim,y_lsim(:,1),'-
g','LineWidth',2),xlabel('Time(sec)'),ylabel('v[ft/sec]')
title('Response to control surfaces 3,4 for impulse input')
subplot(5,1,2)
plot(t_lsim,y_lsim(:,2),'-
g','LineWidth',2),xlabel('Time(sec)'),ylabel('p[rad/sec]')
subplot(5,1,3)
plot(t_lsim,y_lsim(:,3),'-
g','LineWidth',2),xlabel('Time(sec)'),ylabel('r[rad/sec]')
subplot(5,1,4)
plot(t_lsim,y_lsim(:,4),'-
g','LineWidth',2),xlabel('Time(sec)'),ylabel('\phi[rad]')
subplot(5,1,5)
plot(t_lsim,y_lsim(:,5),'-
g', 'LineWidth',2),xlabel('Time(sec)'),ylabel('\psi[rad]')
%%
% Plotting response for control surfaces 5 and 6 for unit impulse input %
And then the next thing is to simulate the results as the following:
u_imp_ail(indx_t_1:indx_t_2,1) = 0*pi/180; % construct impulse input in [RAD]
```

```matlab
u_imp_rud(indx_t_1:indx_t_2,1) = 1*pi/180; % construct impulse input in [RAD]
u_imp_flap(indx_t_1:indx_t_2,1) = 0*pi/180; lat_sys = ss(A,B,C,D);

[y_lsim, t_lsim] = lsim(lat_sys,[u_imp _ail u_imp_rud u_imp_flap],t); %
store all outputs for further investigation
figure,
subplot(5,1,1)
plot(t_lsim,y_lsim(:,1),'-
g','LineWidth',2),xlabel('Time(sec)'),ylabel('v[ft/sec]')
title('Response to control surfaces 5,6 for impulse input')
subplot(5,1,2)
plot(t_lsim,y_lsim(:,2),'-
g','LineWidth',2),xlabel('Time(sec)'),ylabel('p[rad/sec]')
subplot(5,1,3)
plot(t_lsim,y_lsim(:,3),'-
g','LineWidth',2),xlabel('Time(sec)'),ylabel('r[rad/sec]')
subplot(5,1,4) g','LineWidth',2),xlabel('Time(sec)'),ylabel('\phi[rad]')
subplot(5,1,5)

plot(t_lsim,y_lsim(:,4),'-
plot(t_lsim,y_lsim(:,5),'-
g','LineWidth',2),xlabel('Time(sec)'),ylabel('\psi[rad]')
%  Plotting response for control surfaces 7 and 8 for unit impulse input %
And then the next thing is to simulate the results as the following:
u_imp_ail(indx_t_1:indx_t_2,1) = 0*pi/180; % construct impulse input in [RAD]
u_imp_rud(indx_t_1:indx_t_2,1) = 0*pi/180; % construct impulse input in [RAD]
u_imp_flap(indx_t_1:indx_t_2,1) = 1*pi/180;
lat_sys = ss(A,B,C,D);
[y_lsim, t_lsim] = lsim(lat_sys,[u_imp _ail u_imp_rud u_imp_flap],t); %
store all outputs for further investigation
figure,
subplot(5,1,1)
plot(t_lsim,y_lsim(:,1),'-
g','LineWidth',2),xlabel('Time(sec)'),ylabel('v[ft/sec]')
title('Response to control surfaces 7 and 8 for impulse input')
subplot(5,1,2)
plot(t_lsim,y_lsim(:,2),'-
g','LineWidth',2),xlabel('Time(sec)'),ylabel('p[rad/sec]')
subplot(5,1,3)
plot(t_lsim,y_lsim(:,3),'-
g','LineWidth',2),xlabel('Time(sec)'),ylabel('r[rad/sec]')
subplot(5,1,4)
plot(t_lsim,y_lsim(:,4),'-
g','LineWidth',2),xlabel('Time(sec)'),ylabel('\phi[rad]')
subplot(5,1,5)
plot(t_lsim,y_lsim(:,5),'-
g','LineWidth',2),xlabel('Time(sec)'),ylabel('\psi[rad]')
```